1-1-2006

The microbial weathering of uranyl phosphate minerals.

Christina M. Smeaton
University of Windsor

The Microbial Weathering of Uranyl Phosphate Minerals

by

Christina M. Smeaton

A Thesis
Submitted to the Faculty of Graduate Studies and Research
through the Great Lakes Institute for Environmental Research
in Partial Fulfillment of the Requirements for
the Degree of Master of Science at the
University of Windsor

Windsor, Ontario, Canada

2006

ISBN: 978-0-494-42318-9

ABSTRACT

The mobility of the uranyl cation, UO_2^{2+}, is of great concern for nuclear waste disposal and ground water contamination. Under circumneutral to alkaline abiotic conditions uranyl species are often complexed by available carbonate and phosphate leading to the precipitation of uranyl phosphate minerals. However, the reactivity and stability of uranyl phosphates in the presence of a natural microbial consortium is yet to be determined. By measuring the rates of anaerobic microbial weathering by *Shewanella putrefaciens* on the uranyl phosphates; synthetic meta-autunite ($Ca[(UO_2)(PO_4)]_2(H_2O)_6$) and natural torbernite ($Cu[(UO_2)_2(PO_4)_2](H_2O)_{10}$) it was possible to assess the corrosion potential of uranyl U(VI) phosphate phases. The results of this study suggest that microbial weathering of uranyl (VI) phosphate minerals is caused by the incongruent dissolution of the mineral phase with emphasis on the preferential cleavage of oxygen-phosphorus bonds driven by the cellular requirements of bacteria.

CO-AUTHORSHIP

The following thesis contains material from a manuscript that will be submitted to Geochemical Transactions in the near future. The manuscript titled "The Microbial Weathering of Uranyl Phosphates" is co-authored by C.M. Smeaton, D.A. Fowle and C.G. Weisener. Laboratory work presented within this thesis was performed by the author, with help and guidance from D.A Fowle and C.G. Weisener.

ACKNOWLEDGEMENTS

This work is dedicated to Dr. Geoff Rayner-Canham who has been my mentor and advocate since my very first physical chemistry class and who never gave up on me.

First of all I would like to acknowledge Dr. Christopher Weisener's continual support and guidance. I would also like to thank Dr. Weisener for taking me under his supervision from the very first day I arrived at GLIER and teaching me so much about geochemistry. I would also like to thank Dr. David Fowle for his guidance and support and for believing in me and accepting me as his student despite my obvious shortcomings as a geomicrobiologist. In addition, I would like to thank Dr. Brian Fryer for his support and patience; J.C. Barrette and Zhaoping Yang for their patience and assistance with ICP-MS analysis and data processing; Dale Brewe at PNC-CAT BM20 beamline at the Advanced Photon Source (APS), Argonne, IL; Dr. Peter Burns and Dr. Karrie-Ann Kubatko from the University of Notre Dame for providing the synthetic autunite; all of my former Fowle lab mates with special thanks to Arne Sturm, Andrew O'Neil and Karla Leslie; my friends with special thanks to Sonia Melançon's superb pep-talking skills, JanJan Kenney, Sandra Ellis and Carrol Hand, Sandra Ellis, Marelene Rayner-Canham and my mother and brothers for their continual support. Lastly, I would like to thank Steve Perrault for his amazing patience and never ending support throughout this past year.

STATEMENT OF ORIGINALITY

I certify that this thesis, and the research to which it refers, are the product of my own work and that any ideas or quotations from the work of other people, published or otherwise, are fully acknowledged in accordance with the standard referencing practices of this discipline. I acknowledge the helpful guidance and support of my supervisors, Dr. Christopher Weisener (University of Windsor) and Dr. David Fowle (University of Windsor).

LIST OF TABLES

LIST OF FIGURES

TABLE OF CONTENTS

CHAPTER 1

INTRODUCTION

THE PROBLEM

Understanding the fundamental biogeochemical processes governing radionuclide transport is a high priority. Uranium is of particular concern due to its toxicity, long half-life (4.5×10^9 years) and potential mobility in the environment (FINCH and MURAKAMI, 1999). Mining, milling and isotopic processing have produced large volumes of highly toxic and radioactive pollution worldwide. In many cases, the storage of these wastes has been compromised thus leading to the contamination of surface water, groundwater and sediments. Therefore, quantifying both abiotic and biotic processes influencing uranium transport has profound implications for the isolation and containment of uranium wastes.

Uranyl phosphate minerals are common in a wide variety of ore deposits and are believed to control uranium concentrations in many groundwaters owing to their low solubilities. However, the reactivity and stability of uranyl phosphate minerals in the presence of native microbial consortium *in situ* or single bacterial strains is yet to be determined. The goal of this study is to examine the effects of a common dissimilatory metal reducing bacteria (*Shewanella putrefaciens*) on the short and long term stability of two uranyl phosphate minerals: synthetic meta-autunite ($Ca[(UO_2)(PO_4)]_2(H_2O)_6$) and natural meta-torbernite ($Cu[(UO_2)(PO_4)]_2(H_2O)_{10}$) under controlled anaerobic laboratory conditions. By measuring the rates of microbial corrosion of natural and synthetic uranyl-phosphate minerals and comparing quantifiable mineral properties (e.g. solubility and composition) it will be possible to assess the corrosion potential of uranyl

phosphate phases and hence determine uranium mobility under these conditions.

BACKGROUND

Understanding the conditions of mineral formation and alteration is an important part of understanding the geochemical behavior of uranium. Uranium mobility is controlled by redox transformations between insoluble uranium (IV) and soluble uranium (VI). The most important uranium mineral in terms of abundance, wide-spread occurrence and economic value is uraninite, UO_2. It is found as an accessory mineral in granitic igneous rocks, pegmatites and aluminous metamorphic host rocks (FINCH and MURAKAMI, 1999). The chemical structure of uraninite closely resembles spent UO_2 nuclear fuel. Therefore, researchers have taken advantage of these structural similarities by using the behavior of uraninite in natural systems as an analogue for long-term behavior of spent nuclear fuel in geological repositories (BURNS, 1999).

At normal pH values and under reducing conditions, uraninite is sparingly soluble in dilute groundwater. However, the solubility increases with temperature and aqueous fluoride (F), chloride (Cl), and carbon dioxide (CO_2) concentrations. Furthermore, where conditions are sufficiently oxidizing, uraninite is mobilized to the uranyl cation, UO_2^{2+} and the mobility is controlled through complexation with available anions such as carbonate and phosphate. However, the mobility of uranium may also be controlled through uranium-bacteria-mineral interactions. The limitations of current chemical based-approaches to uranium contaminated sites has spawned intense interest to develop cost-effective remediation

approaches based upon microbial/uranium interactions for the decontamination of sediments and water (LLOYD and RENSHAW, 2005).

It is well understood that bacteria and other microorganisms can dramatically impact the form and distribution of uranium in the environment (SUZUKI and BANFIELD, 1999). Bacteria are ubiquitous near the earth's surface and in some cases an excess of 10^8 microorganisms can occupy one gram of soil including cell densities of at least one cell per square micron of surface area on some mineral surfaces (SUZUKI and BANFIELD, 1999). Consequently, interactions between uranium and bacteria have been the focus of extensive studies.

These studies have illustrated the bacterial effects of speciation and mobility of uranium though metabolic processes or metabolic-independent processes such as biosorption or intracellular uptake. Metabolic processes include: formation of chelating agents, enzymatic precipitation and enzymatic uranium reduction. Uranyl phosphates are commonly formed through precipitation reactions involving the enzyme phosphatase. The enzyme catalyzes the release of phosphate from the cell wall thereby increasing local phosphate concentrations to super saturated conditions resulting in uranyl phosphate precipitation (SUZUKI and BANFIELD, 1999).

Macaskie et al. (1985), showed enzymatic phosphate precipitation of aqueous uranyl nitrate hexahydrate on flow through columns containing immobilized *Citrobacter sp* (MACASKIE and DEAN, 1985). In fact, 90% of uranium was retained on the column through uranyl phosphate precipitation. Moreover,

Baskanova et al. (1998) illustrated that secondary uranyl phosphate precipitates were efficient for complexing and removing nickel in wastewaters (BASNAKOVA et al., 1998) . An alternative to phosphate precipitation is complexation.

Microorganisms will also affect uranium mobility by altering local redox conditions. Dissimilatory metal reducing bacteria (DMRB) will generate energy for growth by coupling the oxidation of a carbon source (i.e. acetate, glucose etc.) or hydrogen gas to the reduction of a terminal electron accepting (TEA) metal (i.e. U(VI) via the following reaction:

$$CH_3COO^- + 4\ U^{6+} + 4H_2O \rightarrow 4U^{4+} + 2HCO_3^- + 9H^+$$

$$H_2 + UO_2^{2+} \rightarrow UO_2^0 + 2H^+$$

Bacteria such as *Shewanella putrefaciens*, *Geobacter metallireducens* and *Geobacter sulfurreducens* are widely studied for their ability to reduce aqueous uranyl ions and are used in biogeochemical research as the model bacteria for examining dissimilatory uranium reduction (HAAS and NORTHUP, 2004).

Reductive precipitation into sparingly insoluble uraninite, UO_2, is suggested as an *in situ* remediation tool to immobilize uranium contaminated ground water aquifers. Suzuki et al.(2002), used organic substrates to produce anaerobic conditions to stimulate native bacterial growth in contaminated sediments and groundwater taken from Midnite Mine, Washington (SUZUKI et al., 2002). The dissolved uranium concentration decreased from 20 to 0.3ppm after one month. The authors applied synchrotron based X-ray Absorption near Edge Spectroscopy (XANES) to show the existence of a reduced form of uranium in

the incubated sediment. Furthermore, transmission electron microscope (TEM) images and selected area electron-diffraction (SAED) patterns showed nanoparticles of uraninite associated with the cells. The responsible bacteria was identified through molecular techniques as *Desulfosporosinus spp.* (SUZUKI et al., 2002).

Numerous studies have shown that most uranium uptake by microbes is metabolically independent and it is the nature of the bacterial cell wall polymers that will determine the metal adsorption reactions that will take place (ELIAS et al., 2003; FOWLE et al., 2000; GORMAN-LEWIS et al., 2005; S. D. KELLY et al., 2002; STRANDBERG et al., 1981; SUZUKI and BANFIELD, 1999; SUZUKI et al., 2002). The biosorption of uranium to microbial/algal biomass is commonly utilized in mine site remediation (KALIN et al., 2005). Both gram negative and gram positive cell walls contribute ionizable functional groups as possible metal binding sites. The most common sites are carboxyl, hydroxyl, phosphoryl and amino functional groups. Using geochemical modeling and sorption at low pH values (1.5-5), Fowle et al. (2000) were able to model cell wall sorption with the gram positive bacteria *Bacillus subtillus*. They determined the best fitting model for the uranyl cation was low pH adsorption onto protonated phosphate sites (FOWLE et al., 2000). These observations were later confirmed by synchrotron based Extended X-ray Absorption Fine Structure Spectroscopy (EXAFS) (S. D. KELLY et al., 2002).

While uranium may be sorbed onto cells, it may also accumulate internally. The toxicity of uranium increases the membrane permeability of the

cell and is consequently immobilized by complexation to anionic sites in the cytoplasm or by precipitation (SUZUKI and BANFIELD, 1999; SUZUKI and BANFIELD, 2004). Intracellular accumulation was demonstrated by Suzuki and Banfield (2004) in the inactive cells of *Anthrobacter ilicis*, a common uranium mine isolate. Transmission electron microscope (TEM) images showed intracellular accumulation of uranium that was identified as a uranyl phosphate by energy dispersive spectroscopy (EDS) and selected area electron-diffraction (SAED) patterns.

The research conducted by Suzuki and Banfield (2004) highlights an important factor often overlooked when examining uranium-bacterial interactions. While it is necessary to use well studied and well characterized model bacteria, it is also necessary to use bacteria native to uranium contaminated sites. In the same study the authors examined uranium uptake on inactive *Deinococcus radiodurans* cells isolated from the same mine. *D. radiodurans* is characterized as the most radiation-resistant organism and did not accumulate as much uranium as reported in other studies thus suggesting that uranium accumulation does not correlate directly with resistance. Furthermore, Transmission Electron Microscope (TEM) images, Energy Dispersive X-ray Spectroscopy (EDS) and Single Area Electron Diffraction (SAED) patterns confirmed that *D. radiodurans* precipitated uranyl phosphates extracellularly which is probably the result of phosphate release during cell lysis. It was demonstrated that these inactive cells precipitated uranyl phosphate minerals from a phosphate free solution within 1 hour (SUZUKI and BANFIELD, 2004). This has important implications for uranium

mobility because in many natural oxidizing groundwaters, the precipitation of highly insoluble uranyl phosphate minerals will control aqueous uranium concentrations (FINCH and MURAKAMI, 1999).

Uranyl phosphate minerals form in abundance and have a correspondingly wide distribution in nature thus impacting the mobility of uranium in phosphate-bearing systems. Uranyl phosphates and arsenates constitute the most diverse group of uranium minerals with nearly 70 species described (FINCH and MURAKAMI, 1999). The autunite and meta-autunite subgroup comprises at least 40 of these known mineral species (FINCH and MURAKAMI, 1999; LOCOCK and BURNS, 2003a; LOCOCK and BURNS, 2003b). Autunite group minerals are composed of uranyl phosphate sheets that are connected by interlayer cations and water molecules and are susceptible to dehydration to form meta-autunite minerals (BURNS, 1999; LOCOCK and BURNS, 2003a; SUZUKI et al., 2005b). Members of autunite and meta-autunite groups have a general composition of $A(UO_2PO_4)_2{\cdot}nH_2O$ where A represents a divalent cation and n represents the hydration number (SUZUKI et al., 2005b). These minerals are common in a variety of ore deposits such as the Koongarra Uranium deposit in Australia (FINCH and MURAKAMI, 1999; MURAKAMI et al., 2005; SATO et al., 1997).

Under oxidizing conditions, dissolution of uranium (IV)-bearing minerals such as uraninite mobilize uranium generally due to the formation of uranyl carbonate complexes and in a wide range of uranium deposits the uranyl ions are immobilized into insoluble uranyl phosphates (FINCH and MURAKAMI, 1999; SUZUKI et al., 2005b). In the Koongarra Uranium deposit, iron nodules were

enriched with the copper uranyl phosphate minerals, torbernite and meta-torbernite. The nodules exhibited a higher enrichment of uranium (up to 8 wt%) as compared to other sediments in the deposit (MURAKAMI et al., 2005; SATO et al., 1997). It was suggested that uranium, phosphorus and copper found as trace elements associated with ferrihydrite were released during oxidation and subsequent recrystallization to goethite and hematite. The cations accumulated on the surfaces of the goethite and hematite and continued to coprecipitate nanoparticles of uranyl phosphates during nodule growth (MURAKAMI et al., 2005). Therefore, these iron nodules serves as potential uranium sinks and are important with respect to limiting uranium mobility within the deposit (MURAKAMI et al., 2005; SATO et al., 1997).

Not surprisingly, sites contaminated with uranium from uranium processing plants are also a common location for autunite group minerals to mineralize. Contaminated sediments from former uranium processing facilities in Fernald, Ohio and Hanford in Washington State both show evidence of autunite group mineral formation (CATALANO et al., 2006; FRANCIS and DODGE, 1998). Analysis of contaminated soil from Fernald showed the presence of meta-autunite, uraninite and uranium metaphosphate (FRANCIS and DODGE, 1998). At Hanford, changes in uranium speciation were examined through a depth sequence in a dry former waste pond (CATALANO et al., 2006). While, they did not find variation in uranium speciation they did find variations in uranium mineralogy. At the surface of the pond, uranium was coprecipitated with calcite and at intermediate depths in the vadose zone (3-4m) they found metatorbernite

while at deeper vadose zones the uranium occurred predominantly sorbed onto phyllosilicates. These observations are important with respect to remediation practices at the Hanford Site as the calcite bearing sediments have since been removed from the waste ponds and the fate of uranium within the groundwater will now be determined by torbernite dissolution rates and the desorption of uranium from the phyllosilicates (CATALANO et al., 2006).

In light of the environmental relevance and abundance of uranyl phosphate minerals it is surprising that few studies exist regarding the abiotic and biotic dissolution of the solid mineral phases (KHIJNIAK et al., 2005; SANDINO and BRUNO, 1992; WELLMAN et al., 2006). Sandino and Bruno (1992), examined the dissolution of a synthetic uranyl orthophosphate $(UO_2)_3(PO_4)_2 \cdot 4H_2O$ with respect to phosphate (PO_4^{3-}), hydroxide (OH^-) and carbonate (CO_3^{2-}) complexes. The authors determined that in the pH range (6-9) of natural waters uranyl phosphate complexation will dominate when the total concentration ratio of $[PO_4^{3-}]_T/[CO_3^{2-}]_T$ is greater than 0.1 (SANDINO and BRUNO, 1992).

More recently, Wellman et al. (2006) quantified the effects of dissolved organic material, pH and temperature on the dissolution kinetics of synthetic sodium meta-autunite and natural calcium meta-autunite (WELLMAN et al., 2006). The authors illustrate that meta-autunite dissolution kinetics are strongly dependent on the concentration of dissolved organic material and pH. Dissolved organic material is present in surface water and groundwater and has been shown to complex uranium over a wide range of pH and temperature. The authors used organic TRIS (tris(hydroxymethyl)aminomethane) buffer solutions

to represent dissolved organic material and illustrated that increased TRIS buffer concentrations yielded a higher uranium release from the synthetic sodium meta-autunite.

In both minerals it was shown that while uranium release was affected by pH, phosphorus release rates were not thus supporting the hypothesis that the dissolution of autunite minerals is controlled by a surface mediated reaction with the uranium polyhedra (WELLMAN et al., 2006). It was also shown that the phosphorus release rates were faster than uranium rates by approximately 30 times. At pH 10, an increase of calcium and a decrease in uranium concentrations were observed. Geochemical modeling suggested saturation of calcium and subsequent precipitation of calcium uranate ($CaUO_4$) as the possible mechanism. However, it was shown that the effects of temperature on autunite dissolution up to 70°C were minimal.

Dissolution studies were also conducted in 0.1M deuterated ammonium hydroxide. This study enabled the authors to examine the role that ion exchange with H^+ and the hydronium ion (H_3O^+) played in the dissolution of the mineral. The mean bond enthalpies for H_2O and D_2O are 463.5 and 470.9 kJ/mol, respectively, therefore reflecting a stronger bond for the D_2O compared to H_2O. An observed decrease in the uranium release using D_2O in lieu of H_2O illustrated that uranium release must be governed by the breakage of an O-H (O-D) bond. Therefore, the slower release of uranium into the D_2O is attributed to a rate limiting step in the hydrolysis of uranium within the autunite sheet. The results also showed that uranium release rates were slower in the D_2O while the

phosphorus release rates were not significantly affected. This illustrates that the dissolution of the autunite mineral was controlled by the surface mediated reaction with the uranium polyhedra and release of phosphorus is unaffected by surface mediated reaction. Therefore, these observations supported the hypothesis that dissolution occurs through the surface mediated attack of water at the crystal edges of the autunite sheet and along the cleavage planes (WELLMAN et al., 2006).

Khijniak et al, 2005 reported the only results on the microbial reduction of a uranyl phosphate compound (KHIJNIAK et al., 2005) . They examined the reduction of a biogenically produced uranyl (VI) phosphate phase during the growth of the thermophilic bacterium *Thermoterrabacterium ferrireducens*. This was accomplished by injecting uranyl acetate into a growth medium containing the bacteria. An immediate yellow precipitate was observed and X-ray diffraction analysis identified the phase as a uranyl uramphite ($(NH_4)(UO_2)(PO_4))\cdot 3H_2O$) and 2 later hours it was reduced to ningyoite ($CaU(PO_4)_2\cdot H_2O$). This study is important because it illustrates that the bacteria are able to use the uranium as a terminal electron acceptor even in the presence of the highly insoluble uranyl phosphate mineral phase (KHIJNIAK et al., 2005).

Furthermore, the long term stabilities of bioreduced uranium precipitates are lacking (GINDER-VOGEL et al., 2006; WAN et al., 2005). Wan et al. (2005), showed microbial reoxidation of bioreduced uraninite on contaminated soil columns under strict anaerobic conditions. On day 1, reduced uranium comprised 24% of the original sediment and by day 107, the sediment contained

87% U(IV) thus suggesting successful uranyl bioreduction. However, on day 346, the reduced uranium phase only comprised 58% of the sediment. Wan et al. (2005) suggested that ferric and manganese hydroxides found in sediments served as terminal electron acceptors (TEA). These TEAs coupled with increased carbonate concentrations due to microbial respiration complexed the available uranyl ion thereby increasing the mobility (WAN et al., 2005). This study reaffirms the necessity to conduct long term kinetic studies of remediation and disposal technologies.

While substantial research has examined the microbial reduction of aqueous uranium, there has been limited research investigating the microbial reductive alteration of solid uranium minerals. This study examines the short and long term effects of a metal reducing anaerobic bacteria (*Shewanella putrefaciens*) on solid synthetic meta-autunite $(Ca[(UO_2)(PO_4)]_2\ (H_2O)_6$ and natural torbernite $Cu[(UO_2)_2(PO_4)_2](H_2O)_{10}$ uranyl phosphate minerals under anaerobic laboratory conditions. The goal of this study is to understand the biogeochemical influences that this generic metal reducing bacteria exerts on these solid uranyl mineral substrates and hence its control on uranium mobility.

LITERATURE CITED

Basnakova G., Spencer A. J., Palsgard E., Grime G. W., and Macaskie L. E. (1998) Identification of the nickel uranyl phosphate deposits on *Citrobacter* sp. cells by electron microscopy with electron probe x-ray microanalysis and by proton-induced x-ray emission analysis. *Environmental Science & Technology* **32**, 760-765.

Burns P. C. (1999) The Crystal Chemistry of Uranium. In *Uranium: Mineralogy, Geochemistry and the Environment*, Vol. 38 (ed. P. H. Ribbe), pp. 679. Mineralogical Society of America.

Catalano J. G., McKinley J. P., Zachara J. M., Heald S. M., Smith S. C., and Gordon E. Brown J. (2006) Changes in uranium speciation through a depth sequence of contaminated Hanford sediments. *Environmental Science & Technology* **40**(8), 2517-2524.

Elias D. A., Senko J. M., and Krumholz L. R. (2003) A procedure for quantitiation of total oxidized uranium for bioremediation studies. *Journal of Microbiological Methods* **53**, 343-353.

Finch R. and Murakami T. (1999) Systematics and paragenesis of uranium minerals. In *Uranium: Mineralogy, Geochemistry and the Environment*, Vol. 38 (ed. P. H. Ribbe), pp. 91-179. Mineralogical Society of America.

Fowle D. A., Fein J. B., and Martin A. M. (2000) Experimental study of uranyl adsorption onto *Bacillus subtillis*. *Environmental Science & Technology* **34**, 3737-3741.

Francis A. J. and Dodge C. J. (1998) Remediation of soils and wastes contaminated with uranium and toxic metals. *Environmental Science & Technology* **32**(24), 3993-3998.

Ginder-Vogel M., Criddle C. S., and Fendorf S. (2006) Thermodynamic constraints on the oxidation of biogenic UO_2 by Fe(III) (hydr)oxides. *Environmental Science & Technology* **40**(11), 3544-3550.

Gorman-Lewis D., Elias P. E., and Fein J. B. (2005) Adsorption of Aqueous Uranyl complexes onto *Bacillus subtilis* cells. *Environmental Science Technology* **39**, 4906-4912.

Haas J. R. and Northup A. (2004) Effects of aqueous complexation on reductive precipitation of uranium by *Shewanella putrefaciens*. *Geochemical Transactions* **5**(3), 41-48.

Kalin M., Wheeler W. N., and Meinrath G. (2005) The removal of uranium from mining waste water using algal/microbial biomass. *Journal of Environmental Radioactivity* **78**, 151-177.

Khijniak T. V., Slobodkin A. I., Coker V., Renshaw J. C., Livens F. R., Bonch-Osmolovskaya E. A., Birkeland N.-K., Medvedeva-Lyalikova N. N., and Lloyd J. R. (2005) Reduction of Uranium(VI) Phosphate during Growth of the thermophilic bacterium *Thermoterrabacterium ferrireducens*. *Applied and Environmental Microbiology* **71**(10), 6423-6426.

Lloyd J. R. and Renshaw J. C. (2005) Bioremediation of radioactive waste: radionuclide-microbe interactions in laboratory and field-scale studies. *Current Opinion in Biotechnology* **16**, 254-260.

Locock A. J. and Burns P. C. (2003a) The crystal structure of synthetic autunite, $Ca[(UO_2)(PO_4)]_2(H_2O)_{11}$. *American Mineralogist* **88**, 240-244.

Locock A. J. and Burns P. C. (2003b) Crystal structures and synthesis of the copper-dominant members of the autunite and meta-autunite groups: torbernite, zeunerite, metatorbernite and metazeunerite. *The Canadian Mineralogist* **41**, 489-502.

Macaskie L. E. and Dean A. C. R. (1985) Uranium accumulation by immobilized cells of a *Citrobacter sp. Biotechnology Letters* **7**(7), 457-462.

Murakami T., Sato T., Ohnuki T., and Isobe H. (2005) Field evidence for uranium nanocrystallization and its implications for uranium transport. *Chemical Geology* **221**, 117-126.

S. D. Kelly, Kemner K. M., Fein J. B., Fowle D. A., Boyanov M. I., Bunker B. A., and Yee N. (2002) X-ray absorption fine structure determination of pH-dependent U-bacterial cell wall interactions. *Geochimica et Cosmochimica Acta* **66**(22), 3855–3871.

Sandino A. and Bruno J. (1992) The solubility of $(UO_2)_3(PO_4)_2 \cdot 4H_2O(s)$ and the formation of U(VI) phosphate complexes: Their influence in uranium speciation in natural waters. *Geochimica et Cosmochimica Acta* **56**(12), 4135-4145.

Sato T., Murakami T., Yanase N., Isobe H., Payne T. E., and Airey P. L. (1997) Iron nodules scavenging uranium from groundwater. *Environmental Science & Technology* **31**, 2854-2858.

Strandberg G. W., Shumate S. E., and John R. Parrott J. (1981) Microbial Cells as biosorbents for heavy metals: accumulation of uranium by *Saccharomyces cerevisiae* and *Pseudomonas aeruginosa*. *Applied and Environmental Microbiology* **41**(1), 237-245.

Suzuki Y. and Banfield J. F. (1999) Geomicrobiology of Uranium. In *Uranium: Mineralogy, Geochemistry and the Environment*, Vol. 38 (ed. P. H. Ribbe), pp. 393-432. Mineralogical Society of America.

Suzuki Y. and Banfield J. J. (2004) Resistance to, and accumulation of, uranium by bacteria from a uranium-contaminated site. *Geomicrobiology Journal* **21**, 113-121.

Suzuki Y., Kelly S. D., Kemner K. M., and Banfield J. F. (2002) Nanometre-size products of uranium bioreduction. *Nature* **419**, 134.

Suzuki Y., Sato T., Isobe H., Kogure T., and Muramaki T. (2005) Dehydration processes in the meta-autunite group minerals meta-autunite, metasaléeite, and metatorbernite. *American Mineralogist* **90**, 1308-1314.

Wan J., Tokunaga T. K., Brodie E., Wang Z., Zheng Z., Herman D., Hazen T. C., Firestone M. K., and Sutton S. R. (2005) Reoxidation of bioreduced uranium under reducing conditions. *Environmental Science & Technology* **39**(16), 6162-6169.

Wellman D. M., Icenhower J. P., Gamerdinger A. P., and Forrester S. W. (2006) Effects of pH, temperature, and aqueous organic material on the dissolution kinetics of meta-autunite minerals, $(Na,Ca)_{2-1}[(UO_2)(PO_4)]_2$ $3H_2O$. *American Mineralogist* **91**, 143-158.

CHAPTER 2

The microbial weathering of solid synthetic meta-autunite $Ca[(UO_2)(PO_4)]_2(H_2O)_6$ and natural torbernite $Cu[(UO_2)_2(PO_4)_2](H_2O)_{10}$

INTRODUCTION

The migration of uranium from mining operations and nuclear fuel disposal sites is a major environmental concern. In many cases, improper storage of these wastes has led to the contamination of surface water, groundwater and sediments. Due to the toxicity, long half-life (4.5×10^9 years) and potential mobility in the environment, the mechanisms governing uranium transport is a high priority.(FINCH and MURAKAMI, 1999). Therefore, quantifying both abiotic and biotic processes influencing uranium mobility has profound implications for the isolation and containment of uranium wastes.

The mobility of uranium is controlled by redox transformations between insoluble uranium (IV) and soluble uranium (VI). The most important uranium mineral in terms of abundance, wide-spread occurrence and economic value is uraninite, UO_2. It is found as an accessory mineral in granitic igneous rocks, pegmatites and aluminous metamorphic host rocks (FINCH and MURAKAMI, 1999). The chemical structure of uraninite closely resembles that of spent UO_2 nuclear fuel. Therefore, researchers utilize uraninite as a natural analogue for nuclear fuel to examine long-term behavior in potential geological repositories (BURNS, 1999).

It is well established that bacteria and other microorganisms can dramatically impact the form and distribution of uranium in the environment through non-metabolic and metabolic processes (SUZUKI and BANFIELD, 1999). Dissimilatory metal reducing bacteria (DMRB) will generate energy for growth by coupling the oxidation of an organic food source (ie. acetate, glucose etc.) to the

reduction of a terminal electron acceptor (TEA) such as the uranyl cation (SUZUKI and BANFIELD, 1999). Bacteria such as *Shewanella putrefaciens*, *Geobacter metallireducens* and *Geobacter sulfurreducens* are used in biogeochemical research as model bacteria for examining this process (HAAS and NORTHUP, 2004; KHIJNIAK et al., 2005; Lovley et al., 1991; Lovley and PHILLIPS, 1992; SUZUKI et al., 2002) .

The bioreductive precipitation of uranium (VI) into sparingly insoluble uraninite, UO_2, is widely suggested as an *in situ* remediation tool to immobilize uranium contaminated ground water aquifers. Suzuki et al.(2002), used organic substrates to stimulate native bacterial growth in contaminated sediments and groundwater and produced autunite nanoparticles (SUZUKI et al., 2002). Uranyl phosphate precipitation is suggested as an alternate uranium remediation strategy. Fuller et al. (2002), reported using synthetic hydroxyapatite (Ca_3PO_4), to stimulate the precipitation of uranyl phosphate from solutions. They reported >99.5% removal of the uranyl cation by the hydroxyapatite followed by uranyl phosphate precipitation thus suggesting potential applications in permeable reactive barrier (PRB) remediation technology (FULLER et al., 2002).

Uranyl phosphate minerals form in abundance and have a correspondingly wide distribution in nature thus impacting the mobility of uranium in phosphate-bearing systems. Uranyl phosphates and arsenates constitute the most diverse group of uranium minerals with nearly 70 species described (FINCH and MURAKAMI, 1999). The autunite and meta-autunite subgroup comprises at least 40 of these known mineral species (FINCH and MURAKAMI, 1999; LOCOCK

and BURNS, 2003a; LOCOCK and BURNS, 2003b). Autunite group minerals are composed of uranyl phosphate sheets that are connected by interlayer cations and water molecules and are susceptible to dehydration to form meta-autunite minerals (BURNS, 1999; LOCOCK and BURNS, 2003a; SUZUKI et al., 2005b)

These minerals are common in a variety of ore deposits such as the Koongarra U deposit in Australia (FINCH and MURAKAMI, 1999; MURAKAMI et al., 2005; SATO et al., 1997). Under oxidizing conditions, dissolution of U(IV)-bearing minerals such as uraninite mobilize uranium due to the formation of uranyl carbonate complexes and in a wide range of uranium deposits the uranyl ions are immobilized into insoluble uranyl phosphates (FINCH and MURAKAMI, 1999; SUZUKI et al., 2005b). Not surprisingly, sites contaminated with uranium from processing plants are also a common location for the formation of autunite group minerals. Contaminated sediments from former uranium processing facilities in Fernald, Ohio and Hanford in Washington State both show evidence of autunite group mineral formation (CATALANO et al., 2006; FRANCIS and DODGE, 1998).

In light of the environmental relevance and abundance of uranyl phosphate minerals it is surprising that few studies exist on the dissolution of the solid mineral phases (SANDINO and BRUNO, 1992; WELLMAN et al., 2006). Sandino and Bruno (1992), studied the solubility of a synthetic uranyl orthophosphate $(UO_2)_3(PO_4)_2 \cdot 4H_2O$ and compared the stability to the relative stability of phosphate, hydroxide and carbonate complexes. They determined that in the pH range (6-9) of natural waters uranyl phosphate complexation dominates when

the total concentration ratio $[PO_4^{3-}]_T/[CO_3^{2-}]_T$ is greater than 0.1 (SANDINO and BRUNO, 1992).

More recently, Wellman et al. (2006) quantified the effects of temperature, pH, and dissolved organic material on the dissolution kinetics of synthetic sodium meta-autunite and calcium meta-autunite. Their results showed that meta-autunite dissolution kinetics is strongly dependent on pH and the concentration of dissolved organic material. In both minerals it was shown that while uranium release increases with pH, phosphorus release rates were not thus supporting the hypothesis that the dissolution of autunite minerals is controlled by a surface mediated reaction with the U polyhedra (WELLMAN et al., 2006).

Khijniak et al, 2005 reported the only study of the microbial reduction of a uranyl phosphate compound. They examined the reduction of a biogenic uranyl (VI) phosphate phase formed during the growth of the thermophilic bacterium *Thermoterrabacterium ferrireducens*. The phosphate formed was uranyl uramphite ($(NH_4)(UO_2)(PO_4)\cdot 3H_2O$) and was reduced two hours later to ningyoite ($CaU(PO_4)_2\cdot H_2O$) (KHIJNIAK et al., 2005).

However, there is a dearth of research examining the microbial weathering of uranium phosphate minerals formed prior to inoculation with bacteria. In the present study we examine the short and long term effects of a dissimilatory metal reducing bacteria (*Shewanella putrefaciens*) on solid synthetic meta-autunite $(Ca[(UO_2)(PO_4)]_2\ (H_2O)_6$ and natural torbernite $Cu[(UO_2)_2(PO_4)_2](H_2O)_{10}$ uranyl phosphate minerals under anaerobic laboratory conditions. By measuring the rates of microbial corrosion of natural and synthetic

uranyl-phosphate minerals and comparing quantifiable mineral properties (e.g. solubility and composition) it will be possible to assess the corrosion potential of uranyl phosphate phases and hence determine uranium mobility under these conditions.

MATERIALS and METHODS

A. Mineral Preparation

Synthetic meta-autunite was obtained from P. Burns (University of Notre Dame) and was characterized using X-ray diffraction (XRD) (Figure 1) and scanning electron microscopy (SEM)/ energy dispersive spectroscopy (EDS) (Table 1). The natural torbernite samples were obtained from Old Gunnislake Mine, Gunnislake Cornwall, UK and due to insufficient sample size it was only characterized using SEM/EDS (Table 2) rather then XRD. The synthetic meta-autunite and natural torbernite were placed in dialysis tubing (Spectra/Por® Membrane MWCO: 15,000) and washed daily with 18 MΩ reverse-osmosis-deionized water (Milli-Q) until the supernatant reached pH 7.13 and 6.97 respectively. The samples were removed from the tubing and lypholized.

Both minerals were sieved to a size fraction of 53-125μM. By combining scanning electron microscope (SEM) images and using energy dispersive spectroscopy (EDS)/EDAX® Genesis Particle Analysis Software© the average diameter and surface area of the starting materials was determined based upon 3 random samplings of 68 particles per mineral. The mean diameter (±1σ) of the meta-autunite and torbernite particles was 78.87 ± 0.34 and 90.37 ± 0.49 μm

respectively. The average surface area of the meta-autunite and torbernite was 8104 and 7880 μm^2 respectively.

B. Bacteria and cultivation methods

The strain used in this study, *Shewanella putrefaciens* 200R, was obtained from J. Hass (University of Western Michigan) and chosen based upon its wide use in biogeochemical research as a model bacteria for examining dissimilatory metal reduction. *S. putrefaciens* 200R was originally isolated from a crude oil pipeline in Alberta, Canada (OBUEKWE and WESTLAKE, 1982), and it is a gram-negative, facultatively aerobic bacterium capable of using a broad variety of electron acceptors including uranium (VI) (HAAS and NORTHUP, 2004; LIU et al., 2002).

The cultures were prepared from frozen glycerol stock maintained at -80°C, transferred to Trypticase Soy Agar plates and grown aerobically for 24 hours. Single colonies were inoculated into 20 mL tubes of sterile Trypticase Soy Broth (TSB) and incubated aerobically at 32°C for 18 hours. The 20 mL seed cultures were used to inoculate 100 mL volumes of sterile Luria-Bertrani (LB) media and were incubated aerobically at 32°C until the culture reached late log phase (18 hours).

Bacteria were harvested by centrifugation at 3000 g and washed twice with sterile 0.1M sodium nitrate ($NaNO_3$). Bacteria were also washed twice with aerobic sterile minimal media and once with anaerobic sterile minimal media. The final wet masses of the bacteria in the anaerobic media for the meta-autunite

and torbernite experiments were 1.02 and 1.36g·L^{-1} of minimal media respectively.

The media was degassed in a Coy® anaerobic chamber for 24 hours prior to sterilization to remove dissolved oxygen. Minimal media contained 1.34 mM potassium chloride (KCl), 28 mM ammonium chloride (NH_4Cl), 0.68 mM calcium chloride ($CaCl_2$), 50 mM sodium perchlorate ($NaClO_4$) and 24mM Na-lactate (60% syrup). All experimental media were prepared from reagent grade materials and were either filter sterilized (0.2 μM) or autoclaved.

C. Experimental Methods

The cell suspensions were transferred to the anaerobic chamber (95%N_2/4%H_2) and 15 mL of the suspension was added to 20ml polypropylene test tubes containing 0.001 g of meta-autunite or torbernite. Controls contained 15 mL of sterile experimental media in 20 mL polypropylene tubes containing 0.001g of the meta-autunite or torbernite. There were 88 tubes containing meta-autunite and only 40 tubes containing torbernite due to the small amount of available sample. The samples were rotated end-over-end at 30 rpm and incubated at 30°C in the absence of sunlight.

D. Sampling Methods

Inoculated and control samples were sacrificed over time intervals ranging from 0 to 4.5 months and 0 to 3.5 months for the meta-autunite and torbernite, respectively, with two replicates at each interval. Semi-micro electrodes sterilized with ethanol enabled the monitoring of pH (Thermo Ross Sure-flow semi micro

pH probe) and Eh (Thermo Ross Sure Flow combo redox/ORP) *in situ* before each sampling. Microbial biomass was determined by transferring a 3 mL aliquot of the sample slurry to a 60 mL glass vial containing 7.5 mL of dichloromethane, 15.0 mL of methanol and 5.0 mL of a 5.0 mM phosphate buffer. Lipids were extracted and quantified using the modified Bligh and Dyer procedure (BLIGH and DYER, 1959; WHITE et al., 1979). Glassware was soaked for 24 hours with micro cleaner and placed in a combustion furnace at 500°C in order to prevent lipid contamination. Upon sampling, all vials were covered with foil to minimize photodegradation of lipids.

The concentrations of uranium, phosphorus and copper in the samples were determined using inductively coupled mass spectrometry (ICP-MS). Total uranium was extracted from 0.5 mL of the slurry through acid digestion with trace metal grade 0.1M hydrochloric acid (HCl) followed by filtration through a 0.20 µm nylon syringe filter (ZIELINSKI and MEIER, 1988). Filtered solutions were diluted and acidified with sub-boiling doubly distilled 0.016M nitric acid containing thallium (Tl), beryllium (Be) and Indium (In) as internal standards to correct for instrumental drift and mass bias of the ICP-MS. Dissolved uranium and phosphorus concentrations were determined by filtration of the sample through a syringe coupled with a 0.20 µm nylon syringe filter. Again, filtered samples were diluted and acidified with sub-boiling doubly distilled 0.016M nitric acid containing the Tl/Be/In internal standard. The solid phase was transferred to a microcentrifuge tube and immediately sealed with parafilm to prevent oxygen contamination and placed in a refrigerator at 4°C.

E. Solid Phase Characterization

Field Emission-Environmental Scanning Electron Microscopy (FE-ESEM) (FEI Quanta 200F) was used to characterize the solid phase. Samples were treated with 2.5% gluteraldehyde for 1 hour at room temperature and examined under low vacuum at 10 kV. The abundance and spatial distribution of bacteria with respect to the minerals were examined using backscattered electron (BSE) and secondary electron (SE) detectors. Energy dispersive spectroscopy (EDS) analysis was performed in order to examine any shifts in elemental composition of the minerals. Transmission electron microscopy (TEM) (Phillips 30EM-University of Guelph) was also used to characterize the solid phase in order to view the bacterial cell walls and any mineral phase associations.

F. XANES Experiments

To determine the valence state of the reacted meta-autunite, subset samples of preliminary experiments were collected under similar conditions exhibiting similar solution chemistry. The slurries were syringe filtered in the anaerobic chamber onto 0.45μm filter paper, air dried in the chamber and mounted onto kapton tape to minimize beam effects. The samples were analyzed using X-ray Absorption near edge structures (XANES). The XANES data were collected at the Advanced Photon Source (APS) at Argonne National Laboratory. The samples were run on beamline PNC/XOR BM19 which is capable of an energy range of 2.5-25 keV with a focus beam size of 5μm x 5μm. The uranium absorption edge (U L-III) is 17.16keV, therefore XANES data were collected from 17.1 (pre-edge) to 17.36 (post edges) KeV. Analysis of the

XANES data was performed using Athena version 0.8.05. To determine whether samples were subject to artificial shifts in U reduction as a result of beam induced damage, 4 replicates of data were taken at 3 different locations per filter paper for extended periods of time.

RESULTS and DISCUSSION

Biomass measured within the sample is based on the reasonably strong relationship between phospholipid phosphate (PLP) and microbial carbon content (BLIGH and DYER, 1959; WHITE et al., 1979). Figure 2 illustrates short (A,C) and long term lipid concentrations (B,D) for both the inoculated and control meta-autunite and torbernite. After an initial lipid increase to 72 hours (0.40 $nmol \cdot kg^{-1}$) and 36 hours (0.24 $nmol \cdot kg^{-1}$) for the meta-autunite and torbernite respectively, biomass decreased dramatically in both experiments to near zero values for the rest of the experiment. This suggests the bacterial population was stabilized and decreased to a steady state or death phase. Furthermore, the biomass in the torbernite experiments was significantly lower than the meta-autunite inocula despite a higher initial wet weight of *S. putrefaciens.*

Copper (Cu) toxicity from the torbernite is a potential explanation for the decrease in lipid concentrations. While elements such as copper and nickel play important roles in metabolic processes they can serve as potential toxins to cells at elevated concentrations (SUZUKI and BANFIELD, 1999). Copper will interfere with proteins, enzymatic processes and will weaken the cell membrane (FLEMMING and TREVORS, 1989). In fact, Lovley and Phillips (1992), showed that uranium reduction by *D. desulfuricans* was completely inhibited when 100 μM of

copper (II) was added to solution due to the loss of activity of the cells (LOVLEY and PHILLIPS, 1992).

An alternative explanation for reduced microbial biomass in the torbernite samples is uranium toxicity and radioactivity. While the meta-autunite samples were 99.997% depleted, the torbernite samples showed a moderate radioactivity reading on the Geiger counter. Bacteria are not susceptible to radioactivity because uranium has a long half life as compared to the short life cycles of bacteria (SUZUKI and BANFIELD, 1999). However, the toxicity of uranium may play a role in the reduced biomass. Unlike copper, uranium serves no biological purpose in the cell. Uranium may block essential biological pathways (nutrient transport systems), substitute the essential metal ion from biomolecules, denature enzymes and weaken the cell wall. When we compare the relative U concentrations from EDS measurements we saw that meta-autunite had a higher weight percent of uranium of 50.81% (Table 1) while torbernite (Table 2) had a lower weight percent of 37.35%. Based upon higher relative U concentrations and increased biomass in the meta-autunite samples it may be inferred that U is not toxic to the bacteria in these systems. In fact, back scattered electron (BSE) images and aqueous copper concentrations suggest that copper is inhibiting the growth of the bacteria.

Differences in BSE images were observed between the inoculated torbernite and meta-autunite. The BSE image of the inoculated torbernite showed a lower contrast than the meta-autunite. The production of backscattered electrons varies directly with the specimen's atomic number thus causing higher

atomic number elements to appear brighter than lower atomic number elements. Therefore, due to the high molecular mass (238.0289 $g \cdot mol^{-1}$) of uranium it appears brighter under these conditions. Figures 3A and 3C show BSE images of the control and inoculated torbernite after 2304 hours. The BSE images of the inoculated torbernite appear darker than the control samples (Figure 3A), suggesting a surface masked by lighter elements present on the surface. Bacteria may develop resistance mechanisms to toxic metals through physiological adaptation and a potential mechanism in this case may be the production of bacterial extra cellular polymeric substances (EPS) to sequester the copper (GADD, 2004; SUZUKI and BANFIELD, 1999).

Perhaps the most compelling evidence for the production of EPS is the release of copper over time in the torbernite experiments. Figure 4 shows the initial copper concentration in the inoculated experiments at time zero was 0.25 $\mu mol \cdot L^{-1}$ and after 2880 hours it rose to 1.37 $\mu mol \cdot L^{-1}$ at a rate of 0.022 $\mu mol \cdot L^{-1}$ $hour^{-1}$. While, in the control experiments the initial copper concentration at time zero was 1.18 $\mu mol \cdot L^{-1}$ and after 2880 hours it rose linearly to 4.74 $\mu mol \cdot L^{-1}$ at a rate of 0.0095 $\mu mol \cdot L^{-1}$ $hour^{-1}$. This evidence suggests the bacteria are binding the copper by the formation of EPS as a stress induced response to toxicity. Therefore, the microbial biomass of the bacteria would be lower due to the energy invested to produce the EPS as is seen in the case of the inoculated torbernite samples (Figures 2C and D). Furthermore, the data reveals (Figure 4B) that copper concentrations plateau at 0.22 $\mu mol \cdot L^{-1}$ in the inoculated torbernite until 336 hours where it shows a steep increase to 1.04 $\mu mol \cdot L^{-1}$ at 672

hours followed by another increase to 1.37 $\mu mol \cdot L^{-1}$ at 2880 hours. This suggests the bacteria are beginning to lose their capacity to sequester the copper as illustrated by the rapid decline of bacterial biomass due to cell lysis shown in Figure 2D. An alternative explanation would be the production of copper carbonates commonly formed as a result of increased carbonate (CO_3^{2-}) concentrations due to microbial respiration.

Aqueous uranium release over time in the meta-autunite study is shown in Figures 5A and 5B and illustrates an initial increase of uranium in the inoculated samples with a rate of 0.067 $\mu mol \cdot L^{-1}$ $hour^{-1}$ for the first 42 hours followed by a significant decrease in uranium concentrations (Figure 5A). The highest uranium concentration for the inoculated samples was 3.39 $\mu mol \cdot L^{-1}$ at 12 hours and may be attributed to metabolic activity from the increasing microbial biomass (Figure 2A) coupled with the dissolution of fine grained material on the surface of the meta-autunite. The decrease in aqueous uranium may be due to the formation of an insoluble reduced uranium phase through dissimilatory uranium reduction by *Shewanella putrefaciens* as shown in previous studies (HAAS and NORTHUP, 2004; LIU et al., 2002). Aqueous uranium release over time for the abiotic samples show a minimal initial increase of uranium to 0.43 $\mu mol \cdot L^{-1}$ at 30 hours with a rate of 0.0007 $\mu mol \cdot L^{-1}$ $hour^{-1}$ for the first 42 hours followed by a decrease in uranium concentrations (Figure 5A). This initial release of uranium may be the result of the dissolution of fine grained material on the surface of the mineral as seen with the inoculated samples.

The aqueous release of uranium over time in the torbernite samples is shown in Figures 5C and 5D and illustrates an increase of uranium in the inoculated samples with a rate of 0.00073 $\mu mol \cdot L^{-1}$ hour $^{-1}$ for first 672 hours followed by a decrease in the uranium concentration (Figure 5D). The highest uranium concentration for the inoculated samples was small at 0.075 $\mu mol \cdot L^{-1}$ at 0 hours and may be attributed to the dissolution of fine grained material on the surface of the torbernite. The second largest concentration of aqueous uranium in the inoculated samples was 0.642 $\mu mol \cdot L^{-1}$ at 672 hours, however, at this point the microbial biomass has decreased (Figure 2D), thereby eliminating the potential for dissimilatory uranium reduction in the sample. Aqueous uranium release over time for the abiotic torbernite samples shows a maximum concentration of 1.29 $\mu mol \cdot L^{-1}$ at time 0 followed by a decrease and plateau (Figures 5C and D). The dissolution of fine grained material on the surface of the torbernite is a potential explanation for the initial increase as seen in the abiotic meta-autunite samples.

Figure 6 illustrates extractable total uranium as a function of time. This extraction targets the weakly bound uranium at the mineral and cell surfaces. The highest uranium concentrations for meta-autunite were found at time 0 and were 27.27 $\mu mol \cdot L^{-1}$ for the inoculated sample and 15.58 $\mu mol \cdot L^{-1}$ for the control (Figure 6A,B). While, the highest concentrations for meta-torbernite were 2.54 $\mu mol \cdot L^{-1}$ at 168h for the inoculated sample and 1.93 $\mu mol \cdot L^{-1}$ for the control sample they were still much lower than the meta-autunite values. Again, this

may be the result of the dissolution of fine grained material found on the surface of the minerals.

The difference in chemical structures of the meta-autunite (Figure 7A) and torbernite (Figure 7B) may provide essential insight into the different release rates of uranium. Torbernite contains a single symmetrically independent U(VI) cation that is part of a linear $(UO_2)^{2+}$ cation (LOCOCK and BURNS, 2003b). The uranyl ion is coordinated by four additional oxygen atoms arranged at the equatorial positions of a square bipyramid, with the uranyl ion oxygen atoms at the apices of the bipyramid. Phosphate tetrahedra share the equatorial vertices of uranyl square bipyramids to form the autunite-type sheet, of composition $[(UO_2)(PO_4)]^-$ (LOCOCK and BURNS, 2003a; LOCOCK and BURNS, 2003b). There is a symmetrically independent copper (II) cation in the interlayer between the uranyl phosphate sheets. The copper(II) cation occurs with short bonds to four water groups in a square planar arrangement and two longer bond distances to oxygen atoms of uranyl ions with an interatomic distance of 2.54Å that bridge uranyl phosphate sheets (LOCOCK and BURNS, 2003b) .

While meta-autunite contains the same autunite-type sheet structure as torbernite the interlayer contains the calcium (II) cation that are coordinated by seven water groups. The interatomic distance between the calcium (II) cation and the uranyl ion oxygen atom is 3.275 Å and it is suggested that it may form weak bonds to the autunite sheets. There are two additional H_2O groups that are located in the interlayer where they are held together in position only by hydrogen bonding (LOCOCK and BURNS, 2003a).

The important difference between the two structures with respect to interlayer stability is that within the meta-autunite structure, the calcium (II) cation is only weakly bonded to the uranyl ion via hydrogen bonding while the copper (II) cation in the torbernite forms a stronger covalent bond directly to the oxygen of the uranyl polyhedra. These differences are reflected in the interatomic distances between the cations and the oxygen in the uranyl polyhedra. The interatomic distance between calcium (II) and oxygen in meta-autunite is 3.275 Å. The interatomic distance between copper (II) and oxygen in the torbernite is 2.54 Å (LOCOCK and BURNS, 2003a; LOCOCK and BURNS, 2003b). Therefore, the weak hydrogen bonding within the structure of autunite increases its susceptibility to microbial weathering while the torbernite is more resistant to weathering due to stronger covalent bonding between the oxygen and the uranyl ion. Unfortunately, aqueous calcium release in this study could not be properly quantified due to contribution of the calcium from the 0.68 mM calcium chloride ($CaCl_2$) added to the minimal media.

Furthermore, the interatomic distance of uranium to oxygen within the uranyl polyhedra for torbernite and autunite is 1.79 Å and 2.12 Å respectively, thus implying stronger bonds between the uranium and oxygen in the torbernite thereby reducing its susceptibility to attack and subsequent release of uranium (LOCOCK and BURNS, 2003a; LOCOCK and BURNS, 2003b). Therefore, in light of this evidence coupled with lower microbial biomass observed in the torbernite samples it is not overly surprising that weathering rates are lower in the torbernite experiments.

The release of aqueous phosphorus over time in the inoculated meta-autunite study shows a maximum increase of phosphorous to 95.46 $\mu mol \cdot L^{-1}$ at 30 hours at a rate of 1.35 $\mu mol \cdot L^{-1}$ hour $^{-1}$ during this initial time period followed by a gradual decrease in concentrations at 0.35 $\mu mol \cdot L^{-1}$ hour $^{-1}$ to 1334 hours where the concentrations plateau (Figure 8A and B). The phosphorus released over time in the abiotic samples shows a maximum increase of phosphorous to 57.96 $\mu mol \cdot L^{-1}$ at 12 hours at a rate of 0.689 $\mu mol \cdot L^{-1}$ hour $^{-1}$ during this initial time period followed by a gradual decrease in concentrations to 0.0242 $\mu mol \cdot L^{-1}$ at 1334 hours where the concentrations plateau (Figure 8A and B). The release of aqueous phosphorus over time in the inoculated torbernite samples show a maximum increase of phosphorous at the end of the study of 95.46 $\mu mol \cdot L^{-1}$ at 2880 hours (Figure 8D). However, the steepest increase in phosphorus concentrations during the first 36 hours at a rate of 1.17 $\mu mol \cdot L^{-1}$ hour $^{-1}$ (Figure 8C and D). The rates of aqueous phosphorus release for the abiotic torbernite samples as the concentrations were below the detection limits of the ICP-MS.

The release of phosphorus in the inoculated meta-autunite and torbernite experiments is the strongest indicator of the microbial weathering of the uranyl phosphate minerals. The interatomic distances between the oxygen and the phosphorus bonds are both 1.53 Å therefore the bonds are structurally similar and are susceptible to attack via hydrolysis (Locock and Burns, 2003a; Locock and Burns, 2003b). In fact, the aqueous phosphorus release rates of the meta-autunite and torbernite to 30 hours were both similar at $\mu mol \cdot L^{-1}$ hour $^{-1}$ and 1.17 $\mu mol \cdot L^{-1}$ hour $^{-1}$, respectively. A potential explanation for the initial release of

57.96 $\mu mol \cdot L^{-1}$ of phosphorus in the control meta-autunite (Figure 8C,D) is the abiotic dissolution of the mineral due to the susceptibility of the oxygen-phosphorus bond to hydrolysis. In fact, Wellman et al. (2006), recently showed that abiotic phosphorus release from synthetic and natural autunite increased to as much 30x faster than the dissolution of uranium thus suggesting incongruent dissolution of the mineral, leaving the uranyl polyhedra relatively in tact (WELLMAN et al., 2006).

The increased phosphorus release in the biotic versus abiotic experiments may be explained by the bacterial requirements of phosphorus as an essential element. Bacteria utilize phosphorus for the synthesis of DNA, RNA, ATP, polyphosphates and phospholipids which are made bioavailable in natural systems by the microbial dissolution of highly insoluble phosphate bearing phases such as apatite (JANSSON, 1987). Therefore, breaking the oxygen-phosphorus bond within the uranyl phosphate structure provides bacteria with phosphorus to ensure their survival.

Scanning electron microscope (SEM) images shown in Figure 9 illustrate a gradual comminution of the meta-autunite associated with regions of bacterial attachment which coincides with areas of active high energy sites and a weakening of the mineral matrix. The bottom images are characterized by large fractures along grain boundaries and along cleavage planes. The gradual progression of physical weathering of these minerals coupled with the phosphorus solution chemistry suggests a kinetic reaction driven by the physical

break up of the minerals which may potentially be attributed to the preferential breaking of the oxygen-phosphorus bonds by the bacteria.

In Figure 10 (A,B and C) bacteria and bacterial biomass (10C) are found associated with the meta-autunite mineral. In particular, Figure 10B shows a bacterium associated with a fracture. Generally, fractures have a higher surface area and increase the number of potential reactive sites for bacteria on the surface of the mineral. Therefore, bacteria are commonly found near fractures and fissures on mineral surfaces. Figure 11D illustrates the classic etch pits features commonly associated with bacterial/mineral interactions. The microbial corrosion of meta-autunite also lead to the aggregation of small lathes of uranyl phosphate as in Figure 10. These aggregates are small (5-50μm) thus increasing the surface area and potentially increasing the probability of sorption onto other mineral surfaces or mobility in the environment. TEM images (Figure 12B) reveal polished surfaces of the inoculated meta-autunite lathes with respect to the control, therefore implying weathering of the mineral surface with respect to the control.

EDS/X-ray maps of relative uranium, phosphorus and oxygen concentrations showed a lack of phase difference between the weathered and unweathered areas on the mineral (Figures 13 and 14). The initial increase and subsequent decrease of dissolved uranium in the biotic meta-autunite and torbernite experiments suggests a reduction of uranium (VI) to uranium (IV). However, based on the XANES spectra (Figure 15), there was no observed change in the U L(III) energy absorption edge therefore inferring no detectable

difference in oxidation and implying that the bulk sample has remained as a U(VI) mineral. This observation was also confirmed by SEM images as no secondary mineralization (i.e. uraninite) was detected in any of the samples. However, the absence of detectable uraninite may be due to the limitations of the techniques used. Suzuki et al. (2002), showed nanometre-sized products of uranium bioreduction thus illustrating the need for high resolution microscopy for future investigations of our samples (SUZUKI et al., 2002). In X-ray absorption spectroscopy the detection limit is on the order of a few ppm to 1000 ppm (GALOISY, 2004) and therefore it is possible only a small amount of uraninite was bioprecipitated and bulk x-ray absorption spectroscopy lacked the sensitivity to detect the shift in oxidation state.

The results of this study suggests that a potential model for the microbial weathering of uranyl phosphate minerals may be based upon the incongruent dissolution of the mineral phase with emphasis on the preferential break up of oxygen-phosphorus bonds driven by the cellular requirements of bacteria. Furthermore, substituted cations (i.e. Cu^{2+}) within the uranyl phosphate sheet and crystal structure will have an effect on the rates of uranyl release. It is anticipated that the results from this study may be used as a model for investigating solid uranium mineral microbe interactions.

LITERATURE CITED

Bligh E. and Dyer W. (1959) A rapid method of total lipid extraction and purification. *Canadian Journal of Biochemistry and Physiology* **37**, 911-917.

Burns P. C. (1999) The Crystal Chemistry of Uranium. In *Uranium: Mineralogy, Geochemistry and the Environment*, Vol. 38 (ed. P. H. Ribbe), pp. 679. Mineralogical Society of America.

Catalano J. G., McKinley J. P., Zachara J. M., Heald S. M., Smith S. C., and Gordon E. Brown J. (2006) Changes in uranium speciation through a depth sequence of contaminated Hanford sediments. *Environmental Science & Technology* **40**(8), 2517-2524.

Finch R. and Murakami T. (1999) Systematics and paragenesis of uranium minerals. In *Uranium: Mineralogy, Geochemistry and the Environment*, Vol. 38 (ed. P. H. Ribbe), pp. 91-179. Mineralogical Society of America.

Flemming C. A. and Trevors J. T. (1989) Copper toxicity and chemistry in the environment: a review. *Water, Air & Soil Pollution* **44**, 143-158.

Francis A. J. and Dodge C. J. (1998) Remediation of soils and wastes contaminated with uranium and toxic metals. *Environmental Science & Technology* **32**(24), 3993-3998.

Fuller C. C., Bargar J. R., Davis J. A., and Piana M. J. (2002) Mechanisms of uranium interactions with hydroxyapatite: implications for groundwater remediation. *Environmental Science & Technology* **36**, 158-165.

Gadd G. M. (2004) Microbial influence on metal mobility and application for remediation. *Geoderma* **122**, 109-119.

Galoisy L. (2004) X-ray absorption spectroscopy in geosciences: Information from the EXAFS region. In *Spectroscopic Methods in Mineralogy*, Vol. 6 (ed. A. Beran and E. Libowitzky), pp. 553-587. European Mineralogical Union.

Haas J. R. and Northup A. (2004) Effects of aqueous complexation on reductive precipitation of uranium by *Shewanella putrefaciens*. *Geochemical Transactions* **5**(3), 41-48.

Jansson M. (1987) Anaerobic dissolution of iron phosphorus complexes in sediment due to the activity of nitrate-reducing bacteria. *Microbial Ecology* **14**(1), 81-89.

Khijniak T. V., Slobodkin A. I., Coker V., Renshaw J. C., Livens F. R., Bonch-Osmolovskaya E. A., Birkeland N.-K., Medvedeva-Lyalikova N. N., and Lloyd J. R. (2005) Reduction of uranium(VI) phosphate during growth of the thermophilic bacterium *Thermoterrabacterium ferrireducens*. *Applied and Environmental Microbiology* **71**(10), 6423-6426.

Liu C., Gorby Y. A., Zachara J. M., Fredrickson J. K., and Brown C. F. (2002) Reduction Kinetics of Fe(III), Co(III), U(VI), Cr(VI), and Tc(VII) in cultures of dissimilatory metal-reducing bacteria. *Biotechnology and Bioengineering* **80**(6), 637-649.

Locock A. J. and Burns P. C. (2003a) The crystal structure of synthetic autunite, $Ca[(UO_2)(PO_4)]_2(H_2O)_{11}$. *American Mineralogist* **88**, 240-244.

Locock A. J. and Burns P. C. (2003b) Crystal structures and synthesis of the copper-dominant members of the autunite and meta-autunite groups: torbernite, zeunerite, metatorbernite and metazeunerite. *The Canadian Mineralogist* **41**, 489-502.

Lovley D., Phillips E., Gorby Y., and Landa E. (1991) Microbial reduction of uranium. *Nature* **350**, 413-416.

Lovley D. R. and Phillips E. J. P. (1992) Reduction of Uranium by *Desulfovibrio desulfuricans*. *Applied and Environmental Microbiology* **58**(3), 850-856.

Murakami T., Sato T., Ohnuki T., and Isobe H. (2005) Field evidence for uranium nanocrystallization and its implications for uranium transport. *Chemical Geology* **221**, 117-126.

Obuekwe C. O. and Westlake D. W. S. (1982) Effects of medium composition on cell pigmentation, cytochrome content, and ferric iron reduction. *Canadian Journal of Microbiology* **28**(8), 989-992.

Sandino A. and Bruno J. (1992) The solubility of $(UO_2)_3(PO_4)_2 \cdot 4H_2O(s)$ and the formation of U(VI) phosphate complexes: Their influence in uranium speciation in natural waters. *Geochimica et Cosmochimica Acta* **56**(12), 4135-4145.

Sato T., Murakami T., Yanase N., Isobe H., Payne T. E., and Airey P. L. (1997) Iron nodules scavenging uranium from groundwater. *Environmental Science & Technology* **31**, 2854-2858.

Suzuki Y. and Banfield J. F. (1999) Geomicrobiology of Uranium. In *Uranium: Mineralogy, Geochemistry and the Environment*, Vol. 38 (ed. P. H. Ribbe), pp. 393-432. Mineralogical Society of America.

Suzuki Y., Kelly S. D., Kemner K. M., and Banfield J. F. (2002) Nanometre-size products of uranium bioreduction. *Nature* **419**, 134.

Suzuki Y., Sato T., Isobe H., Kogure T., and Muramaki T. (2005) Dehydration processes in the meta-autunite group minerals meta-autunite, metasaléeite, and metatorbernite. *American Mineralogist* **90**, 1308-1314.

Wellman D. M., Icenhower J. P., Gamerdinger A. P., and Forrester S. W. (2006) Effects of pH, temperature, and aqueous organic material on the dissolution kinetics of meta-autunite minerals, $(Na,Ca)_{2-1}[(UO_2)(PO_4)]_2$ $3H_2O$. *American Mineralogist* **91**, 143-158.

White D., Davis W., Nickels J., King J., and Bobbie R. (1979) Determination of the sedimentary microbial biomass by extractable lipid phosphate. *Oecologia* **40**, 51-62.

Zielinski R. A. and Meier A. L. (1988) The association of uranium with organic matter in Holocene peat: an experimental leaching study. *Applied Geochemistry* **3**, 631-643.

CHAPTER 3

CONCLUSION

CONCLUSION

The ultimate goal of this study was to determine the extent of microbial weathering on the uranyl phosphate minerals meta-autunite and torbernite. The release of phosphorus over time in the inoculated experiments suggests that microbial weathering of uranyl phosphate is driven by the incongruent dissolution of the mineral phase with an emphasis on the preferential breaking of oxygen-phosphorus bonds within the autunite and torbernite structures.

The aqueous release of copper in both the biotic and abiotic experiments illustrates the potential for inner layer cations to be released into the environment. This is particularly important with respect to the potential mobility of other toxic cations that may be found in uranyl phosphates. Furthermore, the potential sequestration of copper by *Shewanella putrefaciens* onto the torbernite mineral surface illustrates a potential sink within uranium contaminated sites that may be susceptible to weathering and remobilization.

The majority of research on uranium-microbial interactions is focused on aqueous uranium biotransformation and in many cases the uranium is reduced to a U(IV) phase such as uraninite (HAAS and NORTHUP, 2004; Lovley et al., 1991; LOVLEY and PHILLIPS, 1992; SUZUKI et al., 2002). However, the results from this study did not suggest bulk uranium reduction which may be the result of limited instrument sensitivity, therefore, solid uranyl phosphate-microbe interactions need to be investigated using highly sensitive techniques. Furthermore, the communition of the mineral and aggregation into smaller particles is also an important observation in terms of the solubility of the uranyl phosphate. While,

uranyl phosphates are generally thought to be insoluble, the BSE showed evidence of substantial weathering. The smaller aggregates hold a greater potential for increased mobility and reactivity within the environment.

In order to improve these studies, it is necessary to utilize surface sensitive surface techniques such as X-ray photoelectron spectroscopy (XPS) and time of flight secondary ion mass spectrometry (TOF-SIMS) to examine localized mineral alterations. XPS will provide compositional and chemical information of the surface atoms (e.g. oxidation state) while TOF-SIMS will provide chemical and compositional information of surface atoms. Depending upon the instrumental conditions the depths can range for TOF-SIMS from a few Å to >100Å. (WEISENER, 2003).

This study should be expanded by examining the microbial weathering of different autunite group minerals. For example, uranyl arsenates have a similar structure to autunite with arsenic occupying the place of phosphorus. Therefore, it would be interesting to examine the microbial weathering rates of these minerals based upon the capacity for arsenic to be a terminal electron acceptor (TEA) for dissimilatory metal reduction (DMR) and the potential mobility and toxicity of arsenic in the environment.

While, *Shewanella putrefaciens* is a model bacteria for examining dissimilatory metal reduction it would be beneficial to use Suzuki and Banfield's approach to examining uranium interactions by using bacteria isolated from an actual uranium mining or contaminated site (SUZUKI et al., 2005a). However, it is important to bear in mind that communities can be misrepresented by

conventional culture dependant sampling techniques (DOJKA et al., 2000; HUGENHOLTZ, 2002). In fact, more than 99% of microorganisms in the environment are unculturable using standard techniques (HUGENHOLTZ, 2002). Therefore, it is necessary to rely on independent culture techniques such as 16S rRNA sequencing and fluorescence *in situ* hybridization (FISH) in order to explore microbial distribution and diversity within uranium contaminated sites (AOI, 2002; DOJKA et al., 2000).

The release of uranium into the environment is the subject of intense public concern and has prompted much research into its fate. However, the results of this study reveal that further work is required in order to accurately characterize the processes on the microbe-mineral scale and it is anticipated that the results from this study will serve as a model to investigate microbe-uranium mineral interactions.

LITERATURE CITED

Aoi Y. (2002) Review: *In situ* identification of microorganisms in biofilm communities. *Journal of Bioscience and Bioengineering* **94**(6), 552-556.

Dojka M. A., Harris J. K., and Pace N. R. (2000) Expanding the known diversity and environmental distribution of an uncultured phylogenetic division of bacteria. *Applied and Environmental Biology* **66**(4), 1617-1621.

Haas J. R. and Northup A. (2004) Effects of aqueous complexation on reductive precipitation of uranium by *Shewanella putrefaciens*. *Geochemical Transactions* **5**(3), 41-48.

Hugenholtz P. (2002) Exploring prokaryotic diversity in the genomic era. *Genome Biology* **3**(2), 00003.1-0.003.8.

Lovley D., Phillips E., Gorby Y., and Landa E. (1991) Microbial reduction of uranium. *Nature* **350**, 413-416.

Lovley D. R. and Phillips E. J. P. (1992) Reduction of uranium by *Desulfovibrio desulfuricans*. *Applied and Environmental Microbiology* **58**(3), 850-856.

Suzuki Y., Kelly S. D., Kemner K. K., and Banfield J. (2005) Direct microbial reduction and subsequent preservation of uranium in natural near-surface sediment. *Applied and Environmental Microbiology* **71**(4), 1790-1797.

Suzuki Y., Kelly S. D., Kemner K. M., and Banfield J. F. (2002) Nanometre-size products of uranium bioreduction. *Nature* **419**, 134.

Weisener C. G. (2003) Novel spectroscopic techniques to characterize mine waste. In *Environmental Aspects of Mine Wastes*, Vol. 31 (ed. R. Raeside), pp. 181-202. Mineralogical Association of Canada.

Table 1. Elemental composition of meta-autunite based upon EDS analysis

Element	Weight %	Atomic Weight %
U	50.81	7.03
O	40.97	84.32
P	7.86	8.36
Ca*	0.36	0.30

*absorption line of Ca is very close to that of uranium therefore there is a potential interference effect

Table 2. Elemental composition of torbernite based upon EDS analysis

Element	Weight %	Atomic Weight %
U	37.35	4.44
O	49.28	87.06
P	5.4	4.98
Cu	7.92	3.52

Figure 1

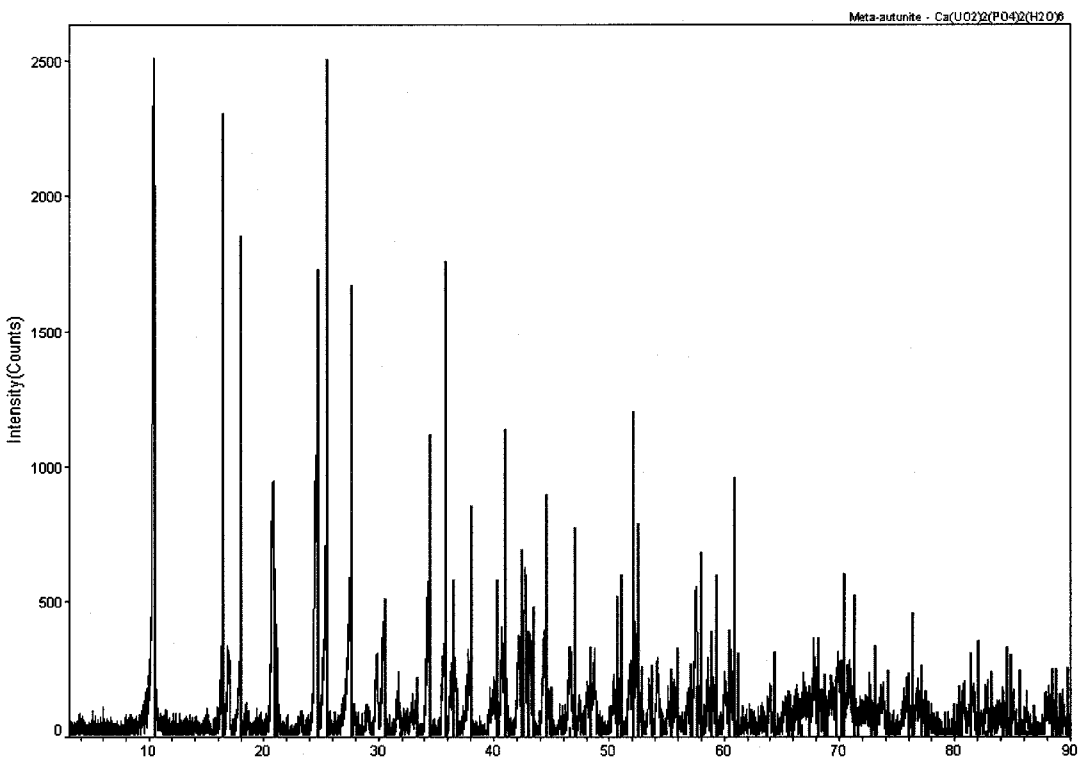

Figure 1: XRD Spectra of synthetic meta-autunite compared to standard spectra (teal)

Figure 2

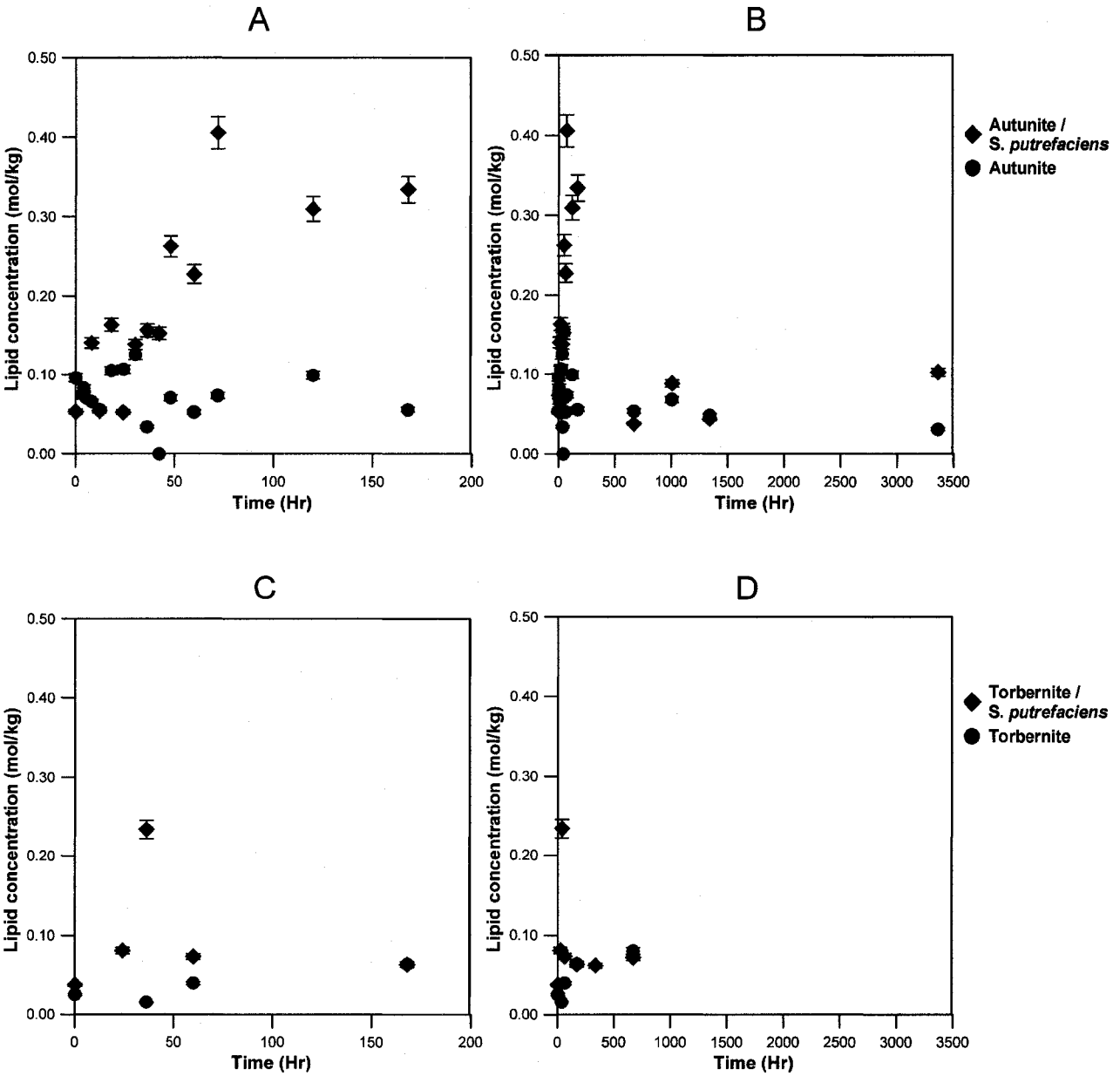

Figure 2 : Lipid concentration (microbial biomass-PLFA) growth as a function of time for the A) synthetic autunite mineral inoculations and autunite controls to 200 hrs B) synthetic autunite mineral inoculations and autunite controls to 3500 hrs C) torbernite mineral inoculations and torbernite controls to 200 hrs and D) torbernite mineral inoculations and torbernite controls to 3500 hrs

Figure 3

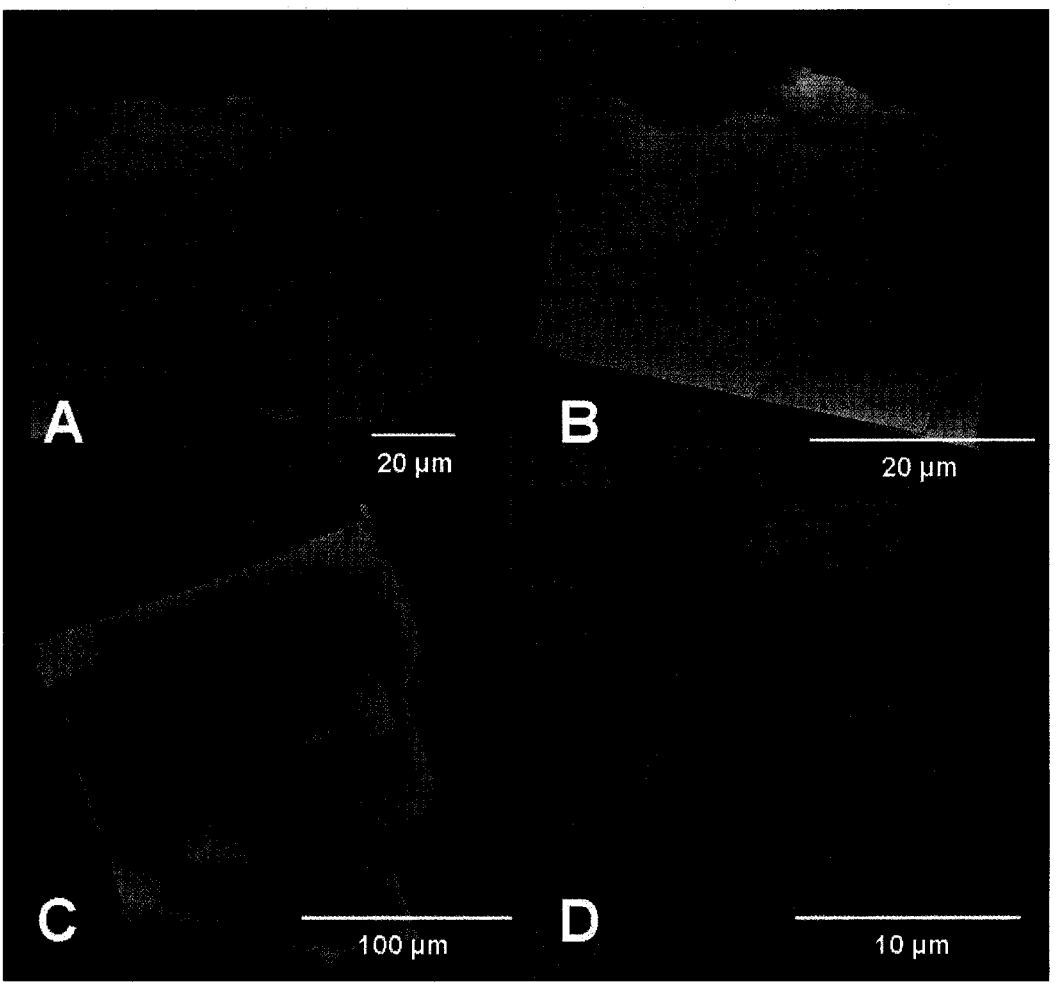

Figure 3: BSE SEM/EDS images at day 96 of A) control torbernite B) and C) inoculated torbernite D) bacterial mineral associations with the torbernite.

Figure 4

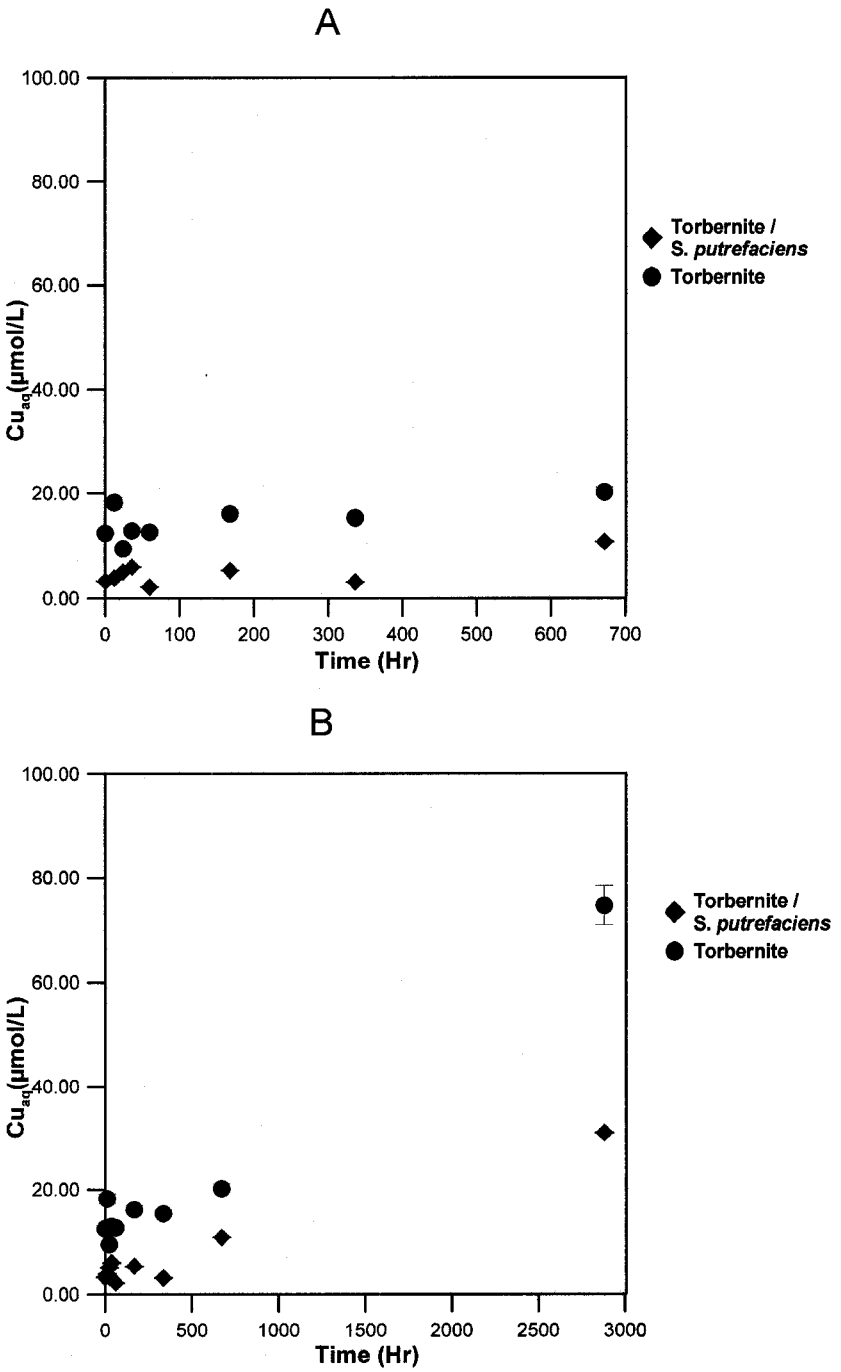

Figure 4 : Aqueous Cu release of A) torbernite mineral inoculations and torbernite controls to 700 hrs and B) torbernite mineral inoculations and torbernite controls to 3500 hrs

Figure 5

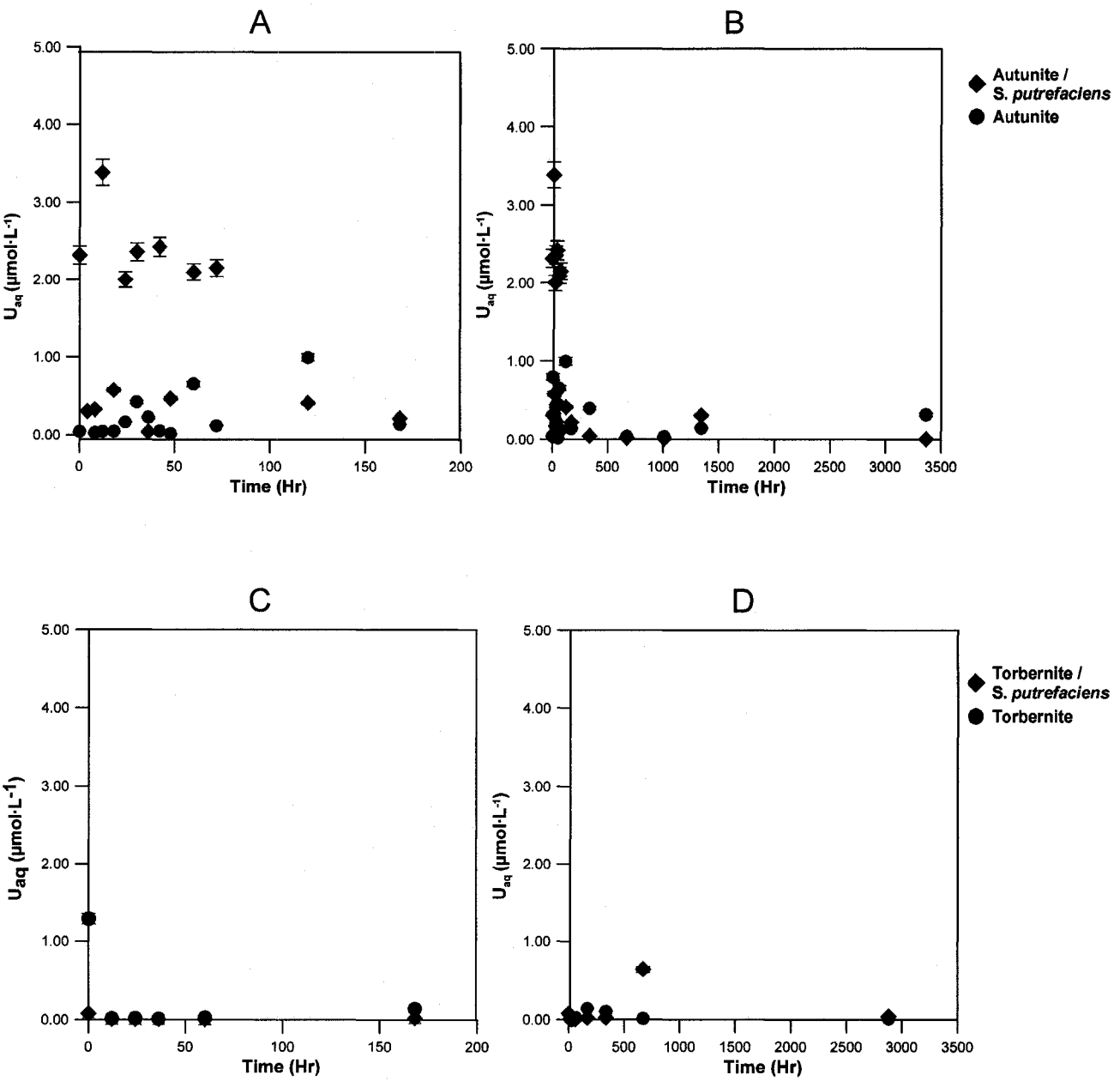

Figure 5: Aqueous U release as a function of time for the A) synthetic autunite mineral inoculations and autunite controls to 200 hrs B) synthetic autunite mineral inoculations and autunite controls to 3500 hrs C) torbernite mineral inoculations and torbernite controls to 200 hrs and D) torbernite mineral inoculations and torbernite controls to 3500 hrs

Figure 6

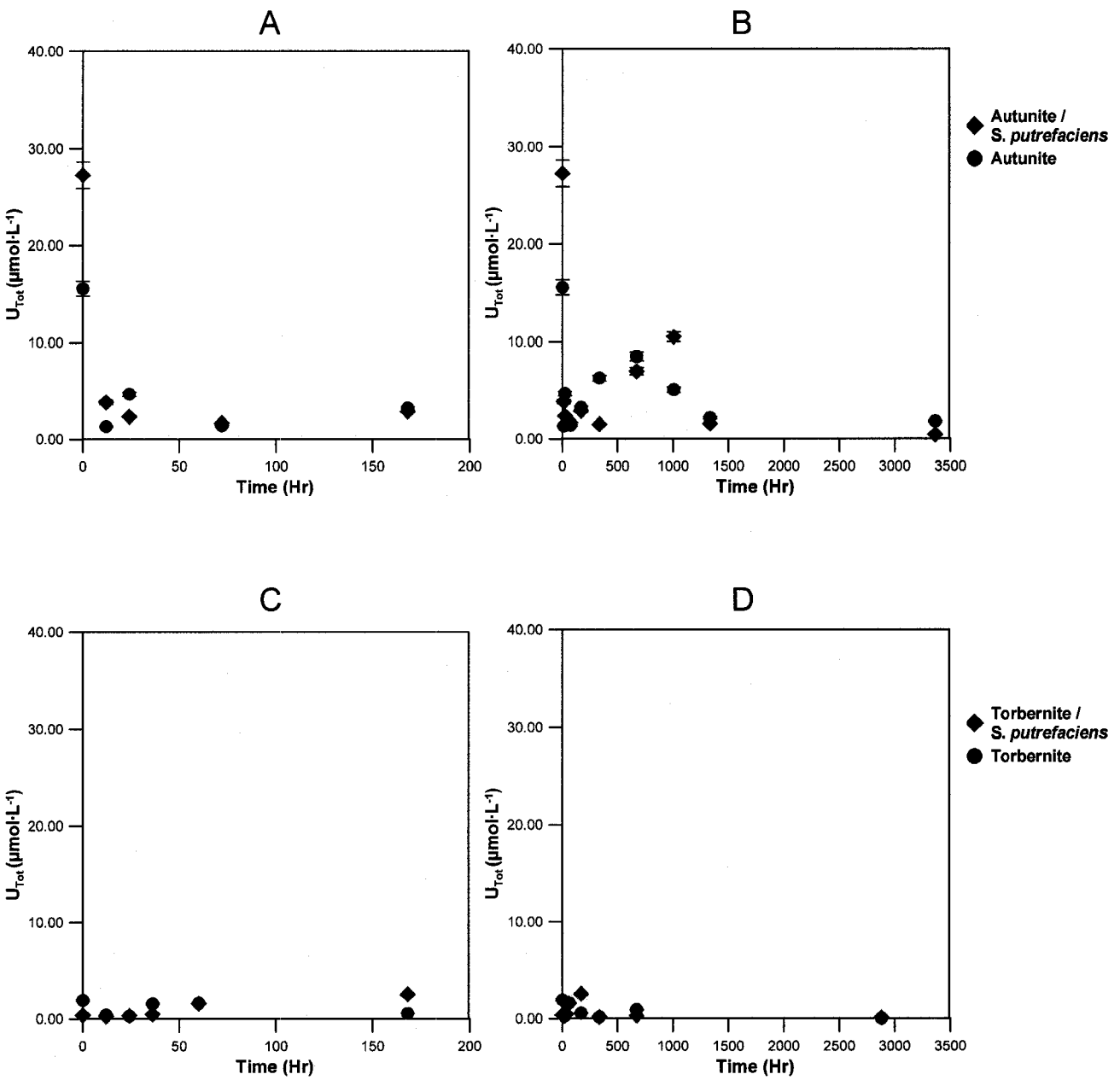

Figure 6 : 0.1M HCL extractable Total U as a function of time for the A)synthetic autunite mineral inoculations and autunite controls to 200 hrs B) synthetic autunite mineral inoculations and autunite controls to 3500 hrs C) torbernite mineral inoculations and torbernite controls to 200 hrs and D) torbernite mineral inoculations and torbernite controls to 3500 hrs

Figure 7

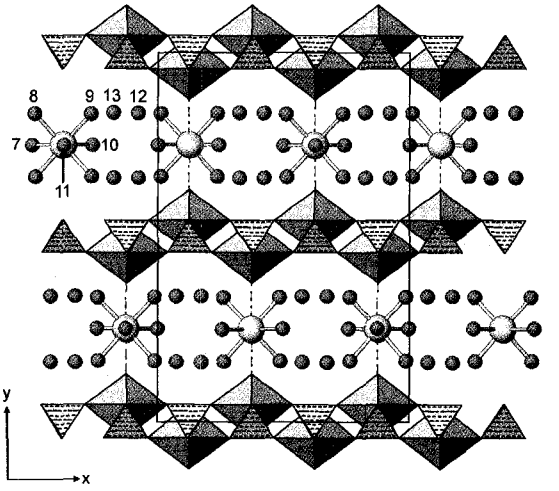

Figure 7A: Polyhedral representation of the structure of autunite, $Ca[(UO_2)(PO_4)]_2\,(H_2O)_6$. *Uranyl polyhedra are shown in gray and the phosphate tetrahedra are stippled. The Ca atoms are shown as large spheres, and the* H_2O *(with O atoms labeled) are shown as small spheres. (*LOCOCK *and* BURNS, *2003a)*

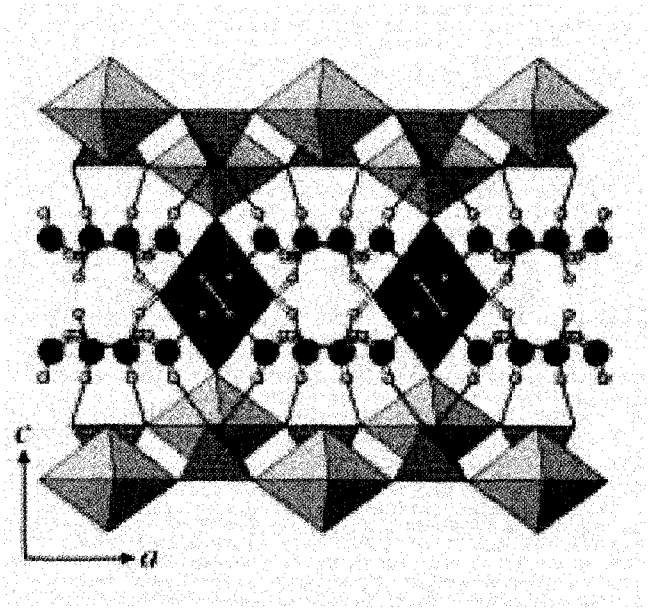

Figure 7B: Polyhedral representation of the structure of torbernite, $Cu[(UO_2)_2(PO_4)_2](H_2O)_{10}$. *Uranyl polyhedra are yellow, phosphate tetrahedra are green and stippled, copper bipyramids are blue, and the* H_2O *groups are shown as red spheres. (*LOCOCK *and* BURNS, *2003b)*

Figure 8

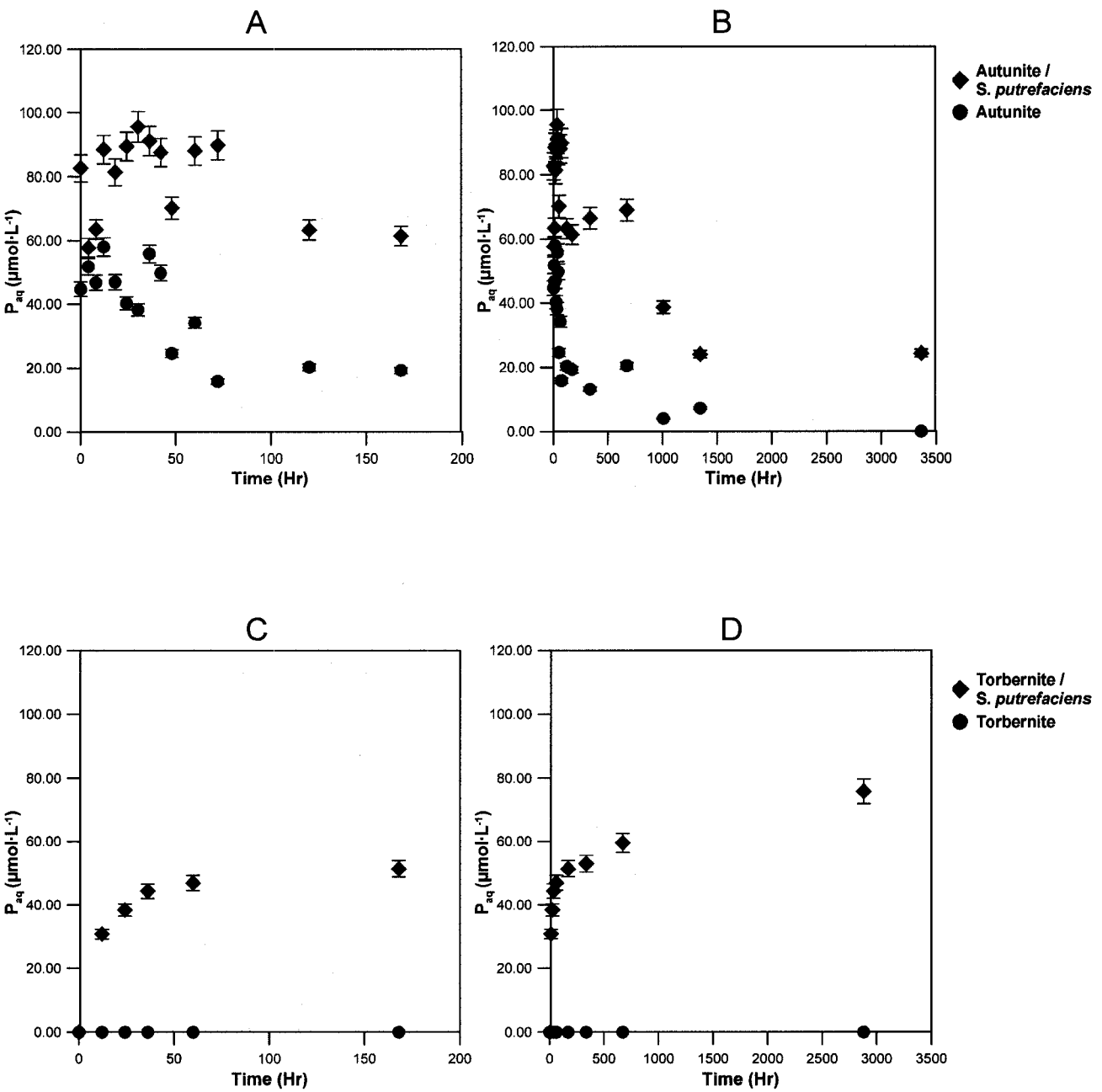

Figure 8: Aqueous P release as a function of time for the A) synthetic autunite mineral inoculations and autunite controls to 200 hrs B) synthetic autunite mineral inoculations and autunite controls to 3500 hrs C) torbernite mineral inoculations and torbernite controls to 200 hrs and D) torbernite mineral inoculations and torbernite controls to 3500 hrs

Figure 9

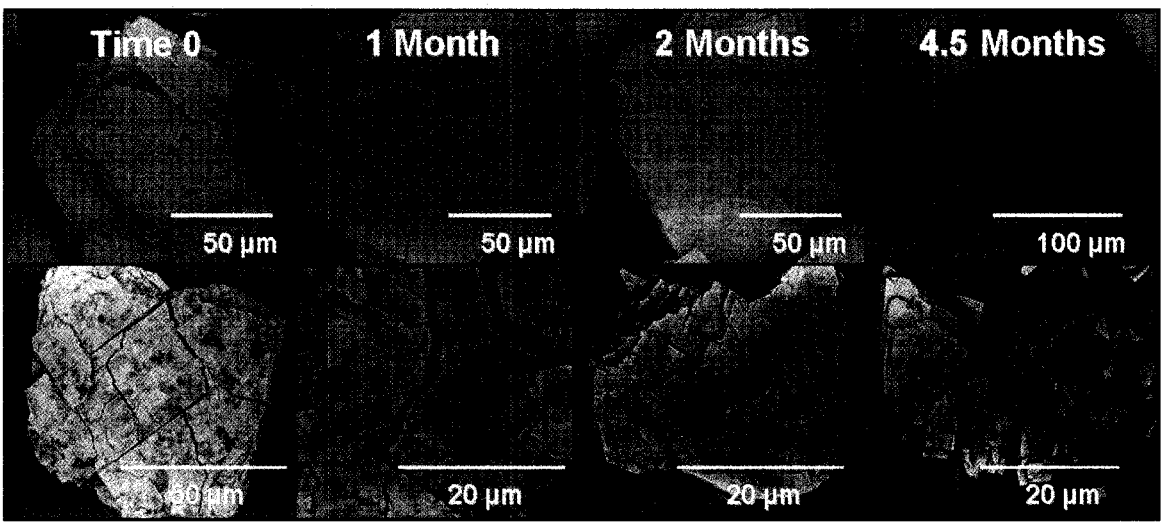

*Figure 9: BSE/SEM images of control autunite minerals (**top**) and inoculated autunite minerals (**bottom**) as a function of time.*

Figure 10

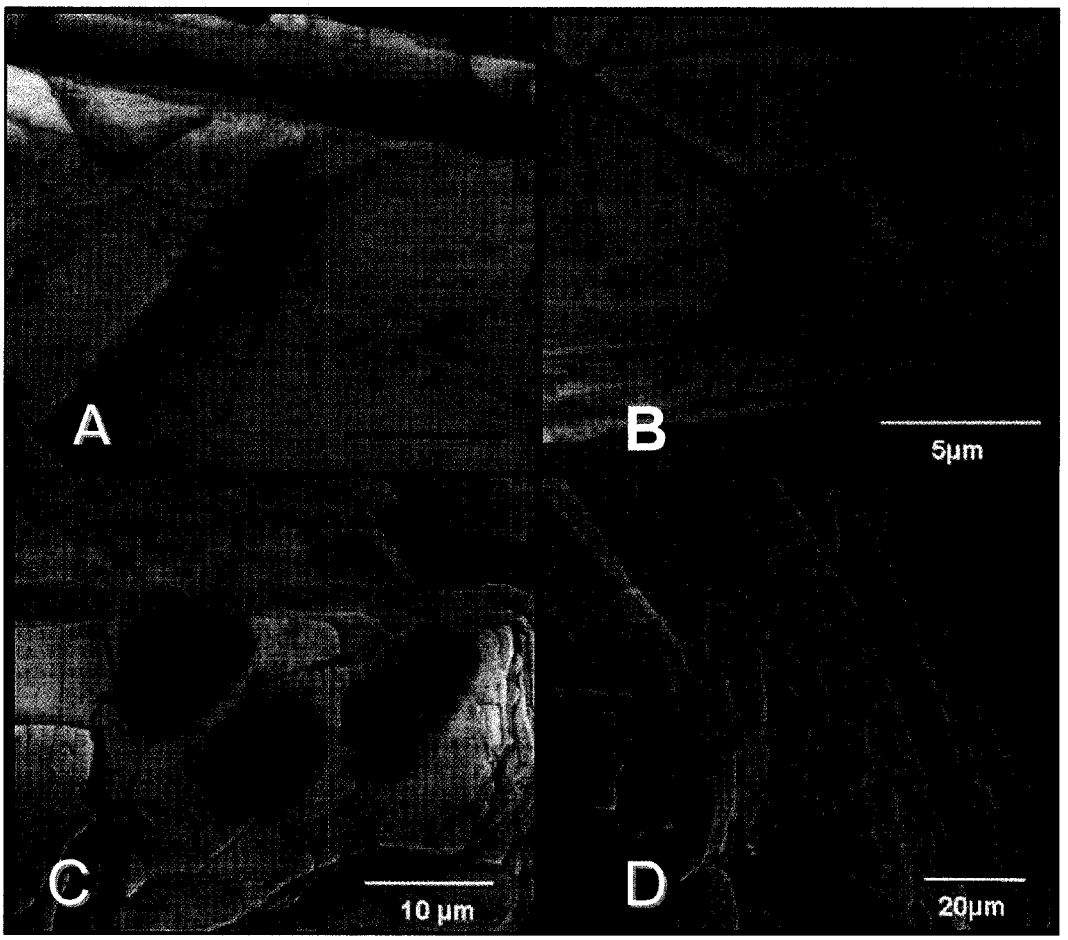

Figure 10: BSE/SEM images of A) S. putrefaciens attached to autunite surface at day 140 with particles associated with cell wall B) Bacteria located an edge site on the meta-autunite after day 1334 C) microbial biomass attached to autunite surface after 140 days embedded with mineral particles D) SE images of etch pits associated with inoculated autunite at day 1008.

Figure 11

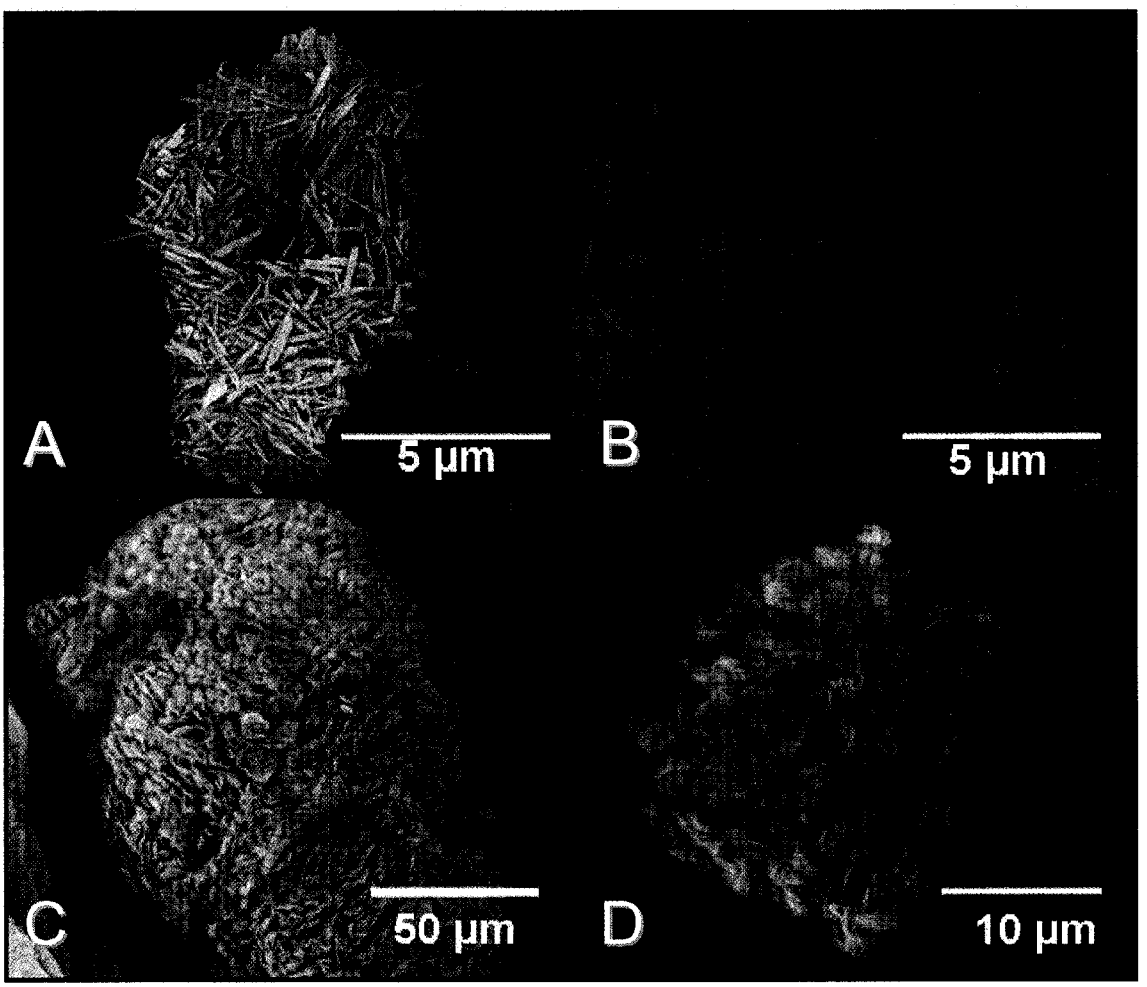

Figure 11: BSE/SEM/EDS images of A,B, C and D) aggregation of the inoculated autunite mineral at day 140

Figure 12

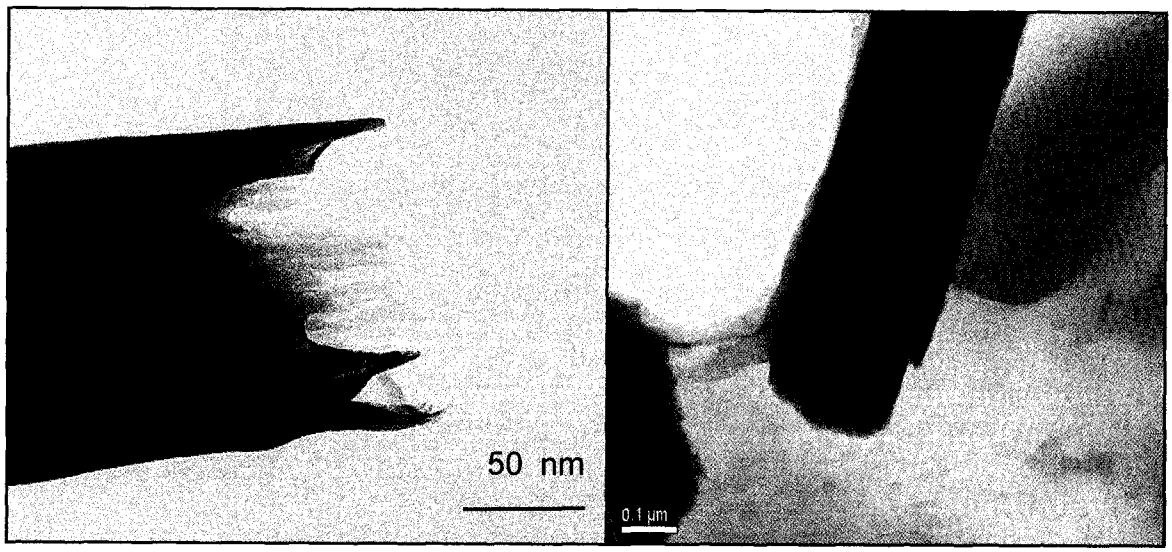

Figure 12 : TEM images of autunite lathes at day 119 of A) autunite control and B) inoculated autunite

Figure 13

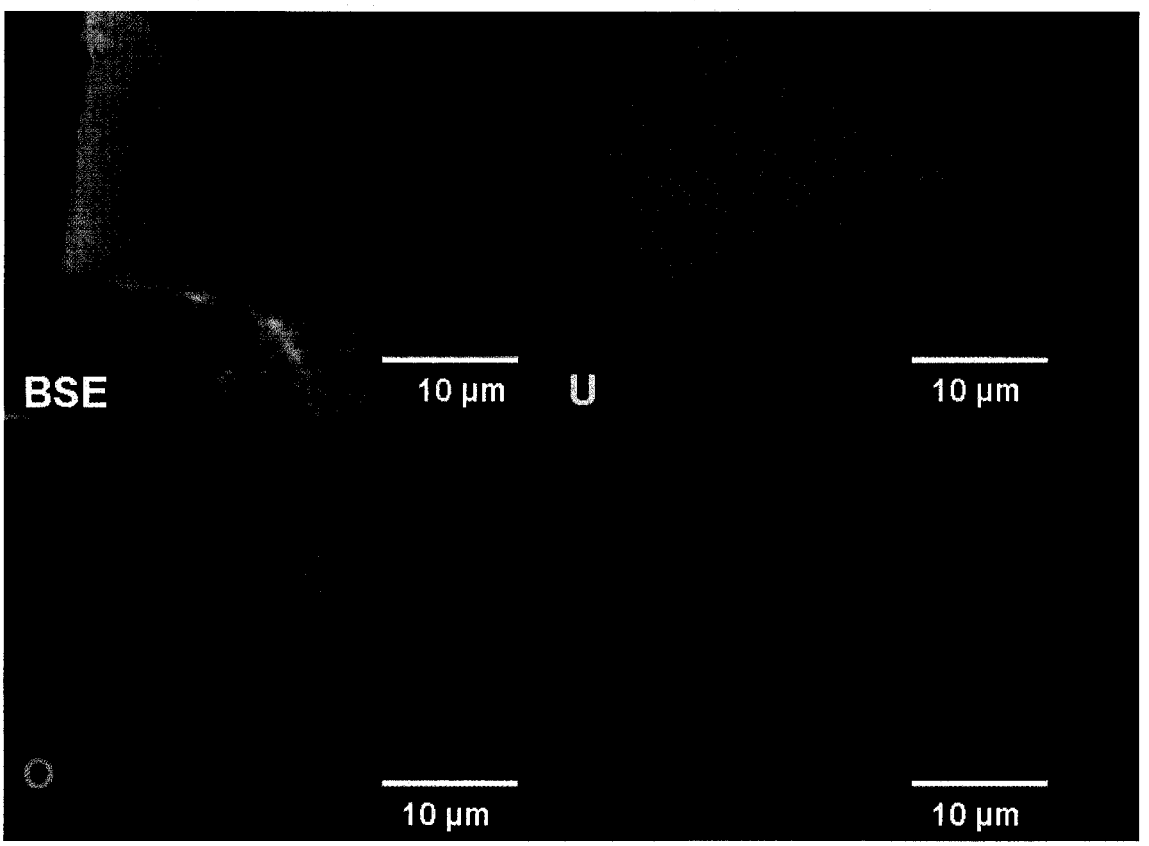

Figure 13 : SEM/EDS X-Ray elemental (U,O and P) map images of inoculated autunite sampled at day 140 (3364 h).

Figure 14

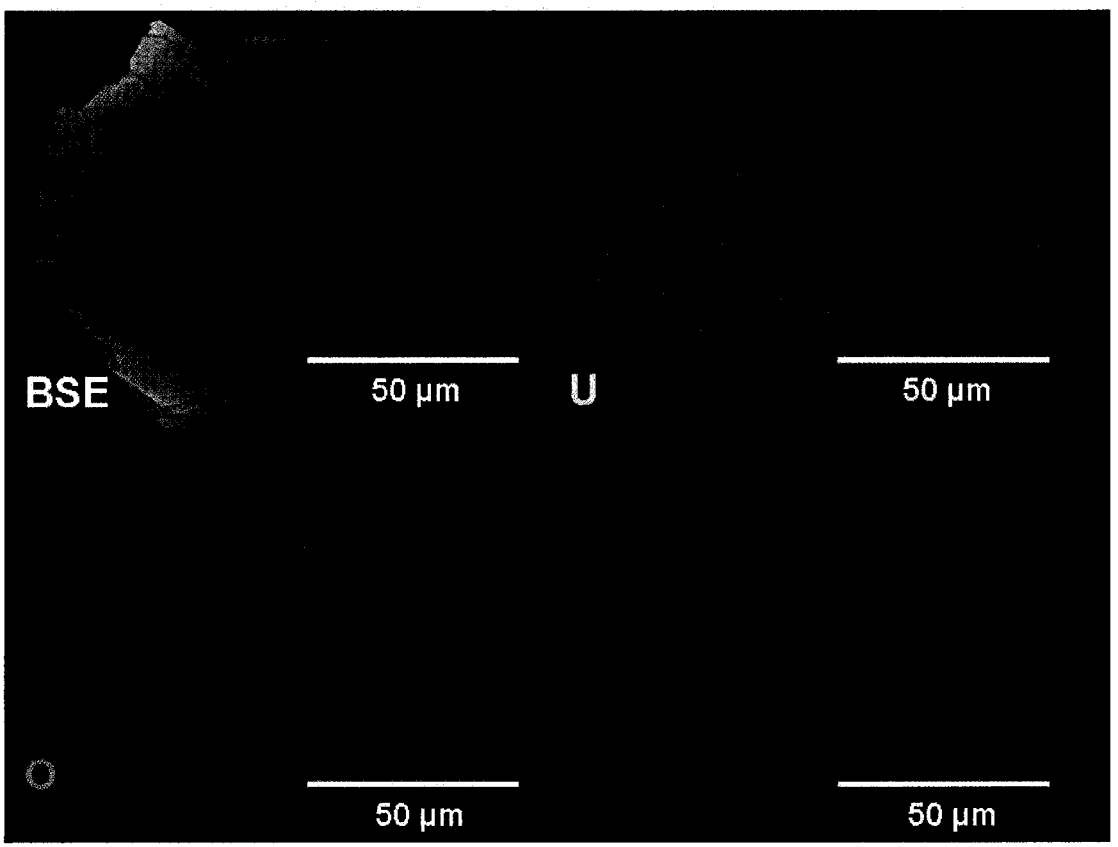

Figure 14 : SEM/EDS X-Ray elemental (U,O and P) map images of inoculated autunite sampled at day 140 illustrating bacterial depletion of U and P associated with the mineral (3364 h).

Figure 15

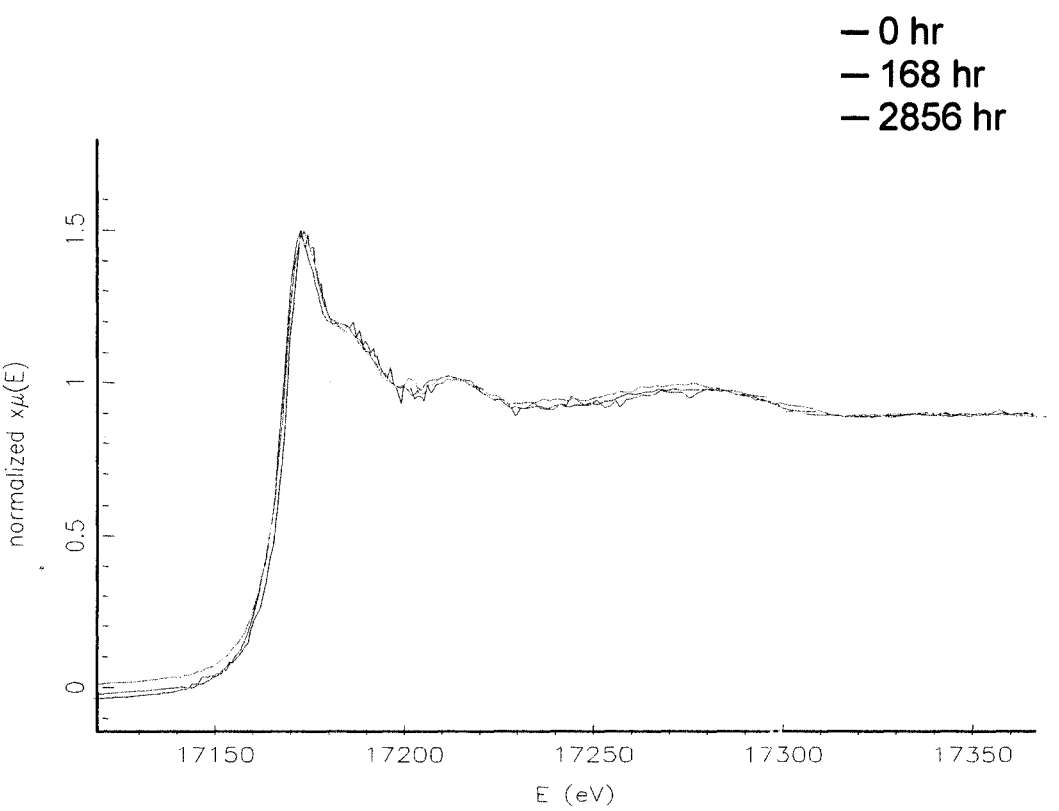

Figure 15: Comparison of U (L III) edges XANES spectra of inoculated autunite mineral at 0,168,2856 hrs